2. EXPLANATORY NOTES[1]

Shipboard Scientific Party[2]

INTRODUCTION

In this chapter, we have assembled information that will help the reader understand the observations on which our preliminary conclusions are based and that also will help the interested investigator select samples for further analysis. This information concerns only shipboard operations and analyses described in the site reports in this Leg 173 *Initial Reports* volume of the *Proceedings of the Ocean Drilling Program.* Methods used by various investigators for shore-based analyses of Leg 173 samples will be described in the individual scientific contributions to be published in the *Scientific Results* volume or elsewhere.

Authorship of Site Chapters

The separate sections of the site chapters were written by the following shipboard scientists (authors are listed in alphabetical order, no seniority is implied):

Site Summary: Beslier, Wallace, Whitmarsh
Background and Objectives: Beslier, Whitmarsh
Operations: Storms, Wallace
Lithostratigraphy: Kudless, Wallrabe-Adams, Wilson
Biostratigraphy: Urquhart, Wise
Paleomagnetism: Turrin, Zhao
Igneous and Metamorphic Petrology: Abe, Beard, Gardien, Hébert, Hopkinson, Rubenach, Skelton, Smith, Wallace
Structural Geology: Froitzheim, Manatschal, Rubenach, Skelton
Core Imaging: Basile, Newton
Organic and Inorganic Geochemistry: Lee, Peng, Wallace
Physical Properties: Takayama, Tompkins, Wilkens
Downhole Measurements: Basile, Louvel, Newton
Summary and Conclusions: Beslier, Whitmarsh
Appendix: Shipboard Scientific Party

Following the site chapters, summary core descriptions ("barrel sheets") and photographs of each core, smear-slide descriptions, sedimentary thin-section descriptions, and igneous thin-section descriptions are included in Sections 3, 4, 5, and 6, respectively (see CD-ROM, back pocket, this volume).

Coring techniques and core handling—including the numbering of sites, holes, cores, sections, and samples—were the same as those reported in previous *Initial Reports* volumes of the *Proceedings of the Ocean Drilling Program*. Following Leg 173, the cores were transferred in refrigerated containers from the ship to cold storage at the Bremen Core Repository of the Ocean Drilling Program in Bremen, Germany.

LITHOSTRATIGRAPHY

The methods of data collection and procedures used to describe and classify sedimentary cores obtained during Leg 173 follow, with only minor modifications, those discussed in the Explanatory Notes for ODP Leg 149, which operated in the same area off western Iberia in 1993 (Shipboard Scientific Party, 1994a). This section, therefore, outlines only those aspects that differ significantly from the practices followed during Leg 149. These include identification of lithostratigraphic units, smear-slide summaries, barrel sheet descriptions using AppleCORE software, and X-ray diffraction analysis.

Identification of Lithostratigraphic Units

At the start of Leg 173 we decided that we would, as far as possible, follow the lithostratigraphic scheme established during Leg 149 for sedimentary cores. However, we did not attempt to establish a lithostratigraphic division at the subunit level that is applicable to all the Leg 149 and 173 sites. Basement units for igneous/metamorphic basement rocks were defined as described in the "Igneous and Metamorphic Petrology" section, this chapter. The following comments summarize the nature of the sedimentary lithostratigraphic units defined during Leg 149 and their occurrence in Leg 173 holes.

The Miocene to Pleistocene turbidite-pelagite sediments of Unit I and the upper part of the Eocene to Miocene carbonate turbidites and hemipelagites of Unit II were not cored during Leg 173. This was because coring commenced only 50–100 m above the estimated depth of acoustic basement. This resulted in coring at all the sites commencing near the base of Unit II. The sediments of Unit II cored in Hole 1065 are early Miocene in age and consist of slumped nannofossil chalks with relatively minor intervals of upward-darkening units (see Fig. 1). This assemblage was not designated as a separate subunit, as it is not similar to any of the previously defined subunits within Unit II. At all the other Leg 173 sites coring commenced near the base of Subunit IIB as defined during Leg 149. The criteria used to define Subunit IIC at Sites 897, 1068, and 1069 are specific to each site, and so the designation "IIC" does not imply that a single lithostratigraphic formation extends across the Leg 149/173 area.

Unit III was encountered at Sites 897 and 899 during Leg 149 (Shipboard Scientific Party, 1994b, 1994c). It consists of brown to reddish brown manganiferous claystones (Subunit IIIA), and red claystones, sands, and conglomerates (Subunit IIIB). It was only encountered in Hole 1070 during Leg 173, where brown manganiferous claystones with thin sand beds and laminae are assigned to Unit III without any division into subunits. Conflicting views concerning the age of this unit are beyond the scope of these explanatory notes; however, it clearly pre-dates the oldest Subunit IIC sediments at Site 897 (middle Eocene) and must be younger than the Aptian-aged Unit IV at Sites 897, 899, and 1067.

Unit IV, defined during Leg 149, consists of Lower Cretaceous mass flow deposits containing a variety of sedimentary lithologies, large boulders of serpentinized mantle, serpentinite breccias, and clasts of other basic igneous rocks. These deposits were interpreted as an olistostrome at Site 897 (Shipboard Scientific Party, 1994b; Comas et al., 1996), and as an olistostrome and/or rock fall deposit at Site 899 (Shipboard Scientific Party, 1994c; Comas et al., 1996; Gibson et al., 1996). During Leg 173, Lower Cretaceous mass flow deposits, showing a variety of features that differ from those previously drilled, were recovered at Sites 1067, 1069, and 1070, and so were also designated as Unit IV. The fact that Unit IV is present at five out of the ten Leg 149 and 173 sites does not indicate that we believe that

[1]Whitmarsh, R.B., Beslier, M.-O., Wallace, P.J., et al., 1998. *Proc. ODP, Init. Repts.*, 173: College Station, TX (Ocean Drilling Program).
[2]Shipboard Scientific Party is given in the list preceding the Table of Contents.

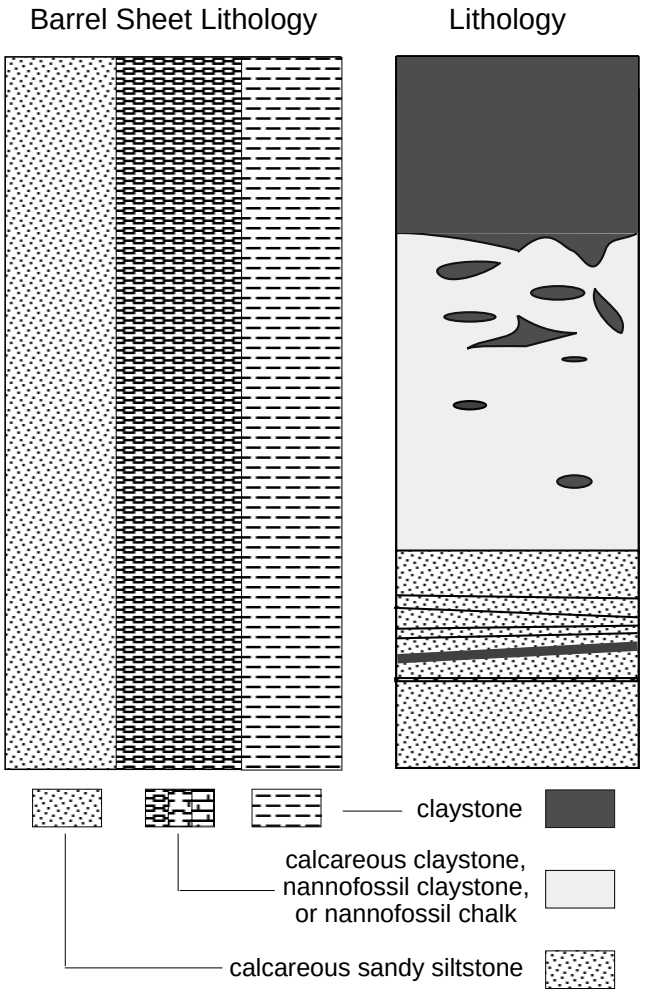

Figure 1. Diagram showing the key features of upward-darkening sequences typical of Unit II recovered in cores from Leg 149 and Leg 173 holes. The lithologies present in the sequences, which are usually between 5 and 15 cm thick, are shown in the right column. The left column shows how the proportion of the lithologies present in the upward-darkening sequences in one core section are depicted on the barrel sheets (see Section 3, this volume). For further discussion, see text under "Lithology."

mass flow deposits of the same age and origin extend continuously across the area.

At Site 901, during the closing hours of Leg 149, a succession of clayey silts with minor calcareous sandstones of Tithonian age was recovered beneath a washed core containing nannofossil clay that yielded Pleistocene to late Aptian ages. Following the normal ODP practice of numbering lithostratigraphic units sequentially downhole, the Tithonian sediments here were designated as Unit II (Shipboard Scientific Party, 1994d). When we encountered a >323-m (?)middle Jurassic to Tithonian succession of clays, claystones, and subsidiary sandstones, and conglomerates beneath Unit II at Site 1065, we designated the Jurassic sediments as Unit V, rather than Unit II as had been done at Site 901, as they are older than Unit IV sediments drilled during Leg 149. Jurassic sediments were also encountered in Hole 1069 and were assigned to Unit V.

Smear Slides and Thin Sections

Smear slides were taken from all major and many minor lithologies, and their texture and composition were determined. Given the subjective nature of smear-slide analysis we did not make percentage estimates of the components present as was done during Leg 149. Instead, relative abundances of different grain types were made on a semiquantitative basis (Rothwell, 1989). Abundances were assigned using the following notation used on Leg 172 (Shipboard Scientific Party, 1998):

Blank = none (not present/found);
T = trace (0%–2%);
R = rare (2%–10%);
C = common (10%–25%);
A = abundant (25%–50%); and
D = dominant (>50%).

Smear-slide and sedimentary thin-section descriptions are included in Sections 4 and 5, respectively (see CD-ROM, back pocket, this volume).

Barrel Sheets

The summary graphic logs and descriptions included in the barrel sheets were based on hand-drawn visual core descriptions (VCDs). Both of these use the ODP sediment classification scheme (Mazzullo et al., 1988) with only slight modification, which is described below under "Lithology." The barrel sheets were drawn at a scale of 1:75 using the AppleCORE software package (version 0.7.5b, 1989–1997). They include the following descriptive columns: Lithology, Bioturbation Intensity, Clast Abundance (when applicable), Physical Structures, Accessories (which include body and ichnofossils), Core Disturbance, Samples, Color, and Remarks. We adopted the definitions/descriptions of these features given in the "Explanatory Notes" chapter of the *Initial Reports* volume for Leg 149 (Shipboard Scientific Party, 1994a), except for "Bioturbation Intensity" and "Clast Abundance," which are described below. The symbols used to represent sediment lithologies, contacts, bioturbation intensity, physical structures, accessories, ichnofossils, and core disturbance are shown in Figure 2.

Lithology

A common lithologic motif observed in sediment cores on this leg and Leg 149 are upward-darkening sequences, usually 5–15 cm thick, consisting of a relatively coarse-grained and light-colored calcareous lithology at the base (e.g., calcareous sandy siltstone), overlain by fine-grained, light-colored calcareous claystone to nannofossil chalk, and capped by dark claystone. To represent this typical three-fold lithology on the barrel sheets, parallel columns of the constituent lithologies of the upward-darkening sequences were used, as shown in Figure 1. The left column represents the basal lithology in the sequence, the central column the middle lithology, and the right column the lithology capping the upward-darkening sequence (typically claystone). The relative widths of the columns on the barrel sheets indicate the relative proportion of each lithology within a series of upward-darkening sequences in each section of core.

The middle lithology in these upward-darkening sequences is quite variable in composition, generally ranging from a calcareous claystone to a nannofossil chalk. We found that color is not a good indicator of composition so it was very difficult to classify the sediments on the basis of their carbonate content. Therefore we chose to describe the middle fine-grained carbonate lithology in the upward-darkening sequences as either calcareous claystone, nannofossil claystone, or nannofossil chalk, omitting any modifiers such as "with clay." We also chose not to use the term "mixed sediment" in describing these lithologies, because such a term is even less precise than the threefold classification of calcareous lithologies that we used. Note that when the middle lithology in the upward-darkening sequences is

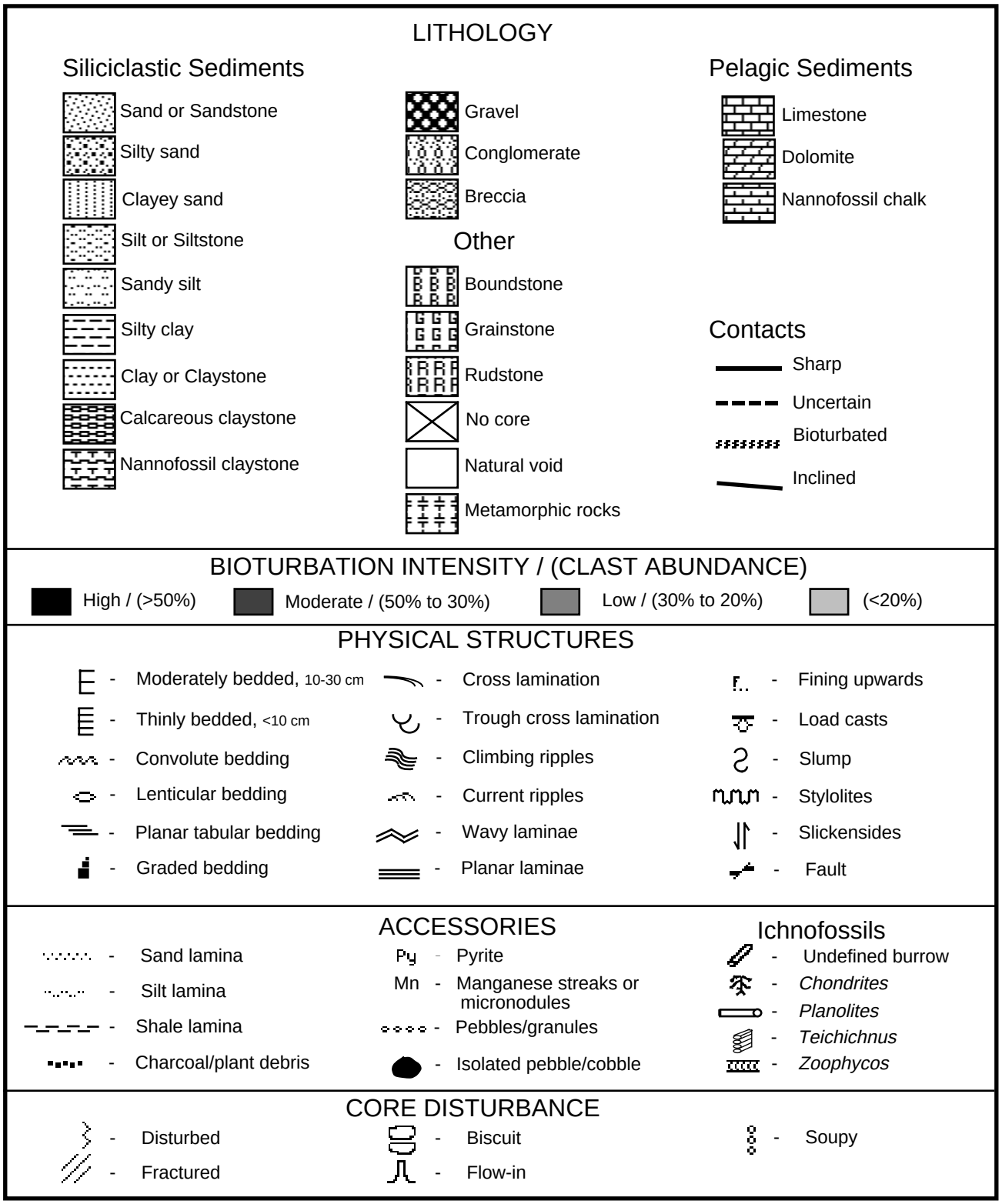

Figure 2. Lithology, contacts, bioturbation intensity, physical structures, accessories, ichnofossils, and core disturbance symbols used in the barrel sheets.

described as "calcareous claystone", the AppleCORE symbol for "calcareous chalk" was used to represent it on the barrel sheets, as shown on Fig. 1. This is because the AppleCORE program does not include a symbol for "calcareous claystone."

Furthermore, because the upward-darkening sequences commonly, but not always, correspond to an upward-fining trend, we have generally indicated upward-darkening sequences with the upward-fining symbol on the barrel sheets. This symbol was placed at the base of individual upward-darkening (upward-fining) sequences.

Bioturbation Intensity

The "Bioturbation Intensity" column of the barrel sheets shows three levels of intensity (Fig. 2):

1. Low: primary sedimentary structures largely intact, and no signs of mottled sediment;
2. Moderate: bioturbation visible as discrete structures. Primary sedimentary structures only moderately disrupted; and
3. High: several generations of bioturbation structures overprinted on each other, resulting in almost total disruption of sedimentary structures, producing a nearly homogeneous sediment.

Where bioturbation intensity is high, it may be difficult to distinguish the apparent absence of structure, caused by bioturbation, from the actual absence of primary structures. Therefore, when the sediment appeared massive and no clear bioturbation or other structures were discernable, the symbol for "low" bioturbation intensity was used, even if we suspected intense bioturbation (e.g., Site 1065, lithostratigraphic Unit II).

Clast Abundance

At Site 1068 a succession of breccias was cored that required the introduction of a new column on the barrel sheets to represent clast abundance in the breccias. This was accomplished by relabeling the column usually shown as "Bioturbation Intensity" to "Clast Abundance" for those cores at Site 1068 in which breccia was recovered. Visual estimates of the proportion of clasts were made using diagrams in Rothwell (1989), and the following four categories were used: <20%, 20%–30%, 30%–50%, and >50%. When >50% clasts are present, the breccia is considered clast supported. On the barrel sheets, the proportion of clasts is represented by light gray to black shading, with the lightest gray indicating <20% clast abundance and black indicating >50% clast abundance.

Samples

The locations of samples taken from each core for shipboard analysis are indicated in the "Samples" column on the barrel sheets. The following notation is used to indicate the purpose of sample collection:

CAR – inorganic and organic carbon analysis;
IW – whole-round interstitial water geochemistry analysis;
PAL – micropaleontology sample;
SS – smear slide;
TSB – thin section;
XRD – X-ray diffraction; and
PH – close-up photograph position.

Color

The hue and chroma attributes of color of the cores are included in the "Remarks" column as Munsell colors (Munsell Color Company, 1971), whereas descriptive color names are recorded in the "Color" column of the barrel sheets. A key to the "Color" column abbreviations is presented in Table 1.

X-ray Diffraction

As far as possible we tried to coordinate sampling for routine X-ray diffraction (XRD) mineral analyses with that for carbonate analyses (see "Organic and Inorganic Geochemistry" section, this chapter) and physical properties (see "Physical Properties" section, this chapter) analyses so that samples for all three analyses were commonly taken adjacent to each other. Qualitative bulk mineralogical XRD analysis was used in combination with thin-section, smear-slide, and carbonate analyses to characterize the mineralogy of representative lithostratigraphic units. XRD diffractograms were analyzed using MacDiff software (MacDiff version 3.2b5 PPC, 1991–1996). The XRD data are archived on the Leg 173 *Initial Reports* CD-ROM (back pocket, this volume) for postcruise interpretation.

BIOSTRATIGRAPHY

Preliminary age assignments were based on biostratigraphic analyses of calcareous nannofossils and planktonic foraminifers. Paleodepth interpretations were based on benthic foraminifers. Calcareous nannofossil datum ages were constrained by examining at least one sample per section of core (with a sample spacing of ~1.5 m). In addition, for a quick initial age estimate, the core-catcher material from every core was also examined for calcareous nannofossil content. Core-catcher material was also examined for planktonic foraminifers and supplemented by additional core samples where necessary. The preservation, abundance, and zonal assignment for each sample and for each microfossil group are recorded in the stratigraphic site summary sheets.

Estimates of biostratigraphic ages were calibrated against the magnetic polarity time scale of Cande and Kent (1995). The time scale of Berggren et al. (1995) was applied to the Cenozoic (Figs. 3–5). Berggren et al. (1995) also provided age estimates for this time interval for both calcareous nannofossil and planktonic foraminifer datums.

The time scale of Gradstein et al. (1995) was used for the Cretaceous and Jurassic together with the stratigraphic framework of Channell et al. (1995), which was used for the Early Cretaceous–

Table 1. Codes for sediment colors used in the barrel sheets.

Intensities		Modifier		Color	
Abbreviation	Meaning	Abbreviation	Meaning	Abbreviation	Meaning
Vlt	Very light	Bl	Bluish	BF	Buff
Lt	Light	Br	Brownish	BK	Black
Mlt	Medium light	Cr	Creamy	BL	Blue
Med	Moderate	Gy	Greyish	BR	Brown
Mdk	Medium dark	Gn	Greenish	CR	Cream
Dk	Dark	Or	Orange	GY	Gray
Vdk	Very dark	Ol	Olive	GN	Green
Vpl	Very pale	Pk	Pinkish	OR	Orange
Pal	Pale	Pu	Purplish	OL	Olive
Dsk	Dusky	Rd	Reddish	PK	Pink
Vds	Very dusky	Wh	Whitish	PU	Purple
Bri	Brilliant	Ye	Yellowish	RD	Red
Viv	Vivid	Mo	Mottled	WH	White
Str	Strong	Sp	Spotty	YE	Yellow
Dp	Deep				
Vdp	Very deep				

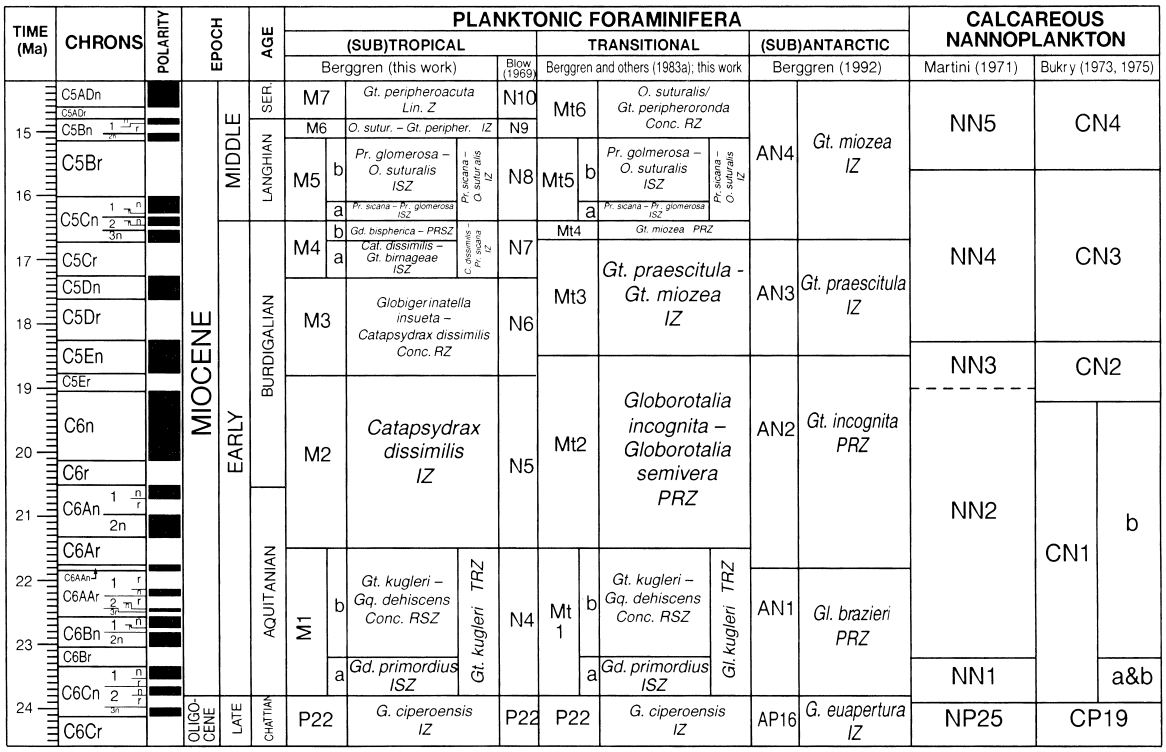

Figure 3. Early Miocene time scale used for this volume (from Berggren et al., 1995).

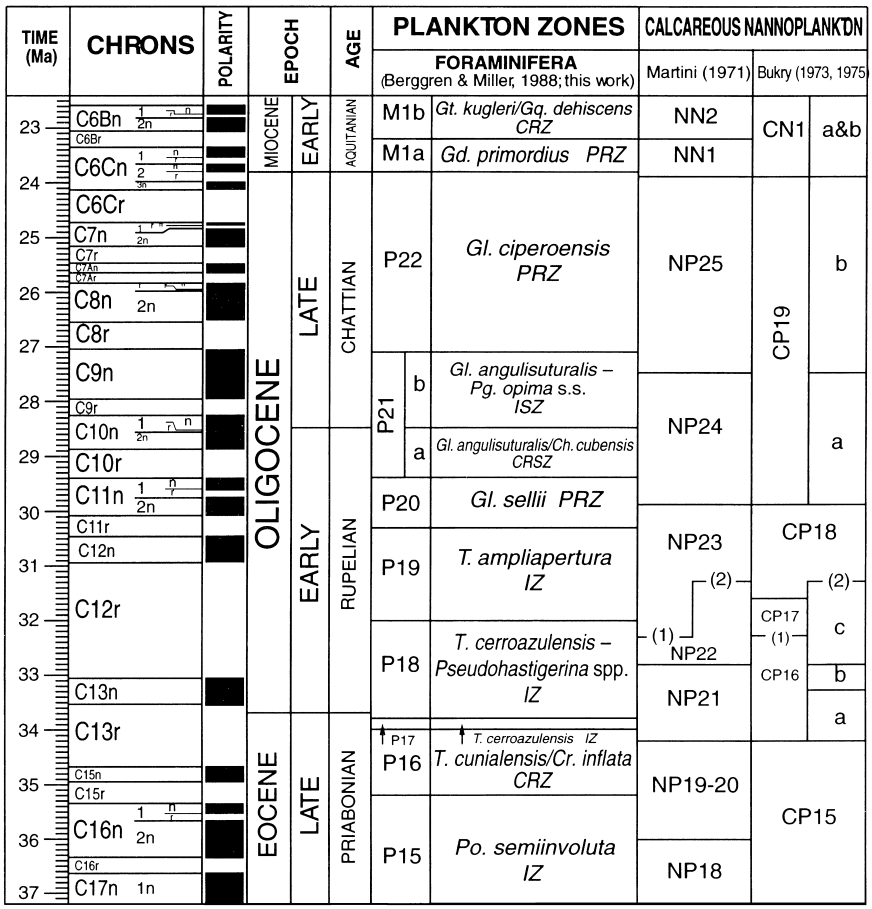

Figure 4. Oligocene time scale used for this volume (from Berggren et al, 1995).

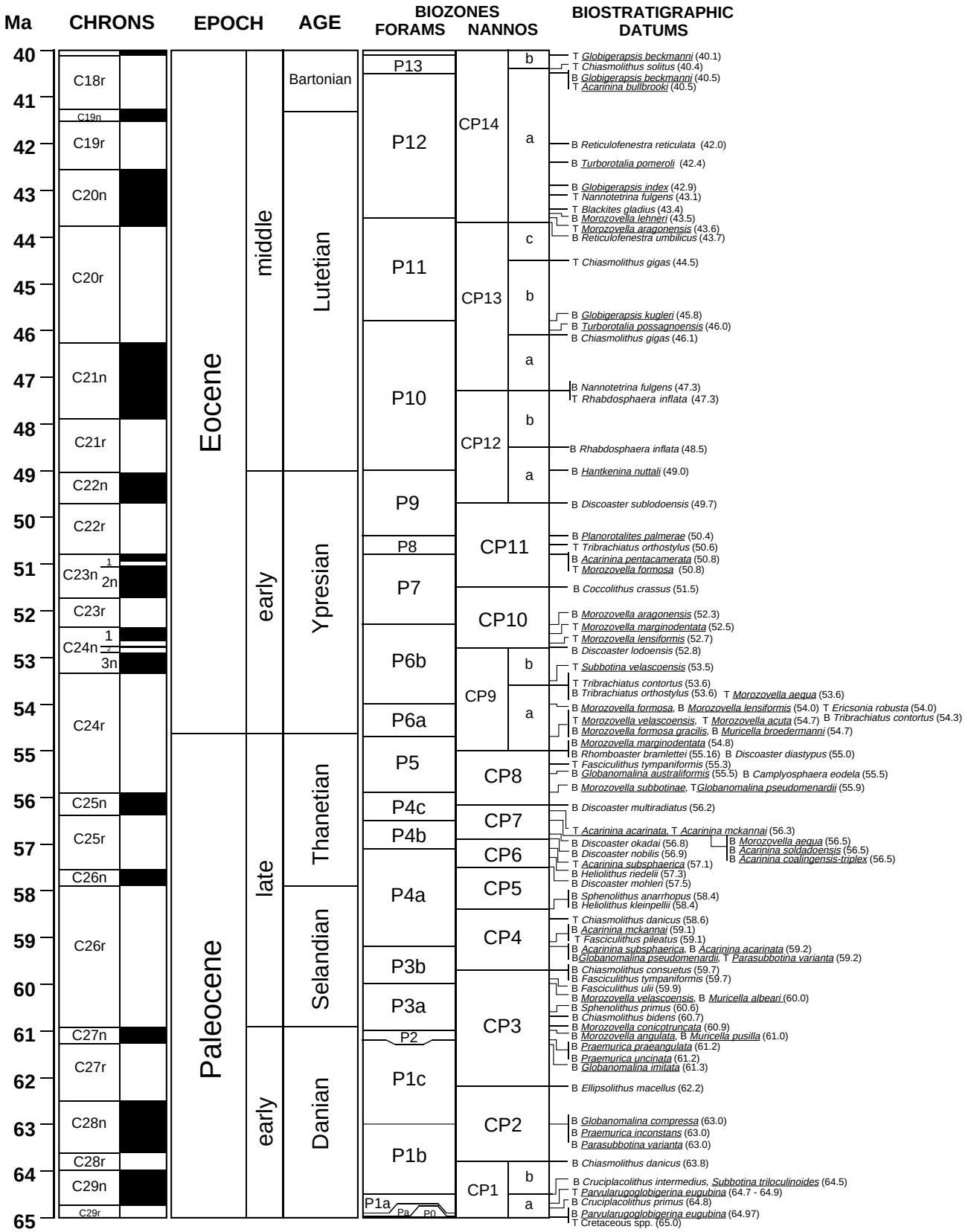

Figure 5. Eocene through Cretaceous time scales and biostratigraphic datums used for this volume (after Berggren et al., 1995; Gradstein et al., 1995; Erba et al., 1995). Foraminifers are underlined; nannofossils are not.

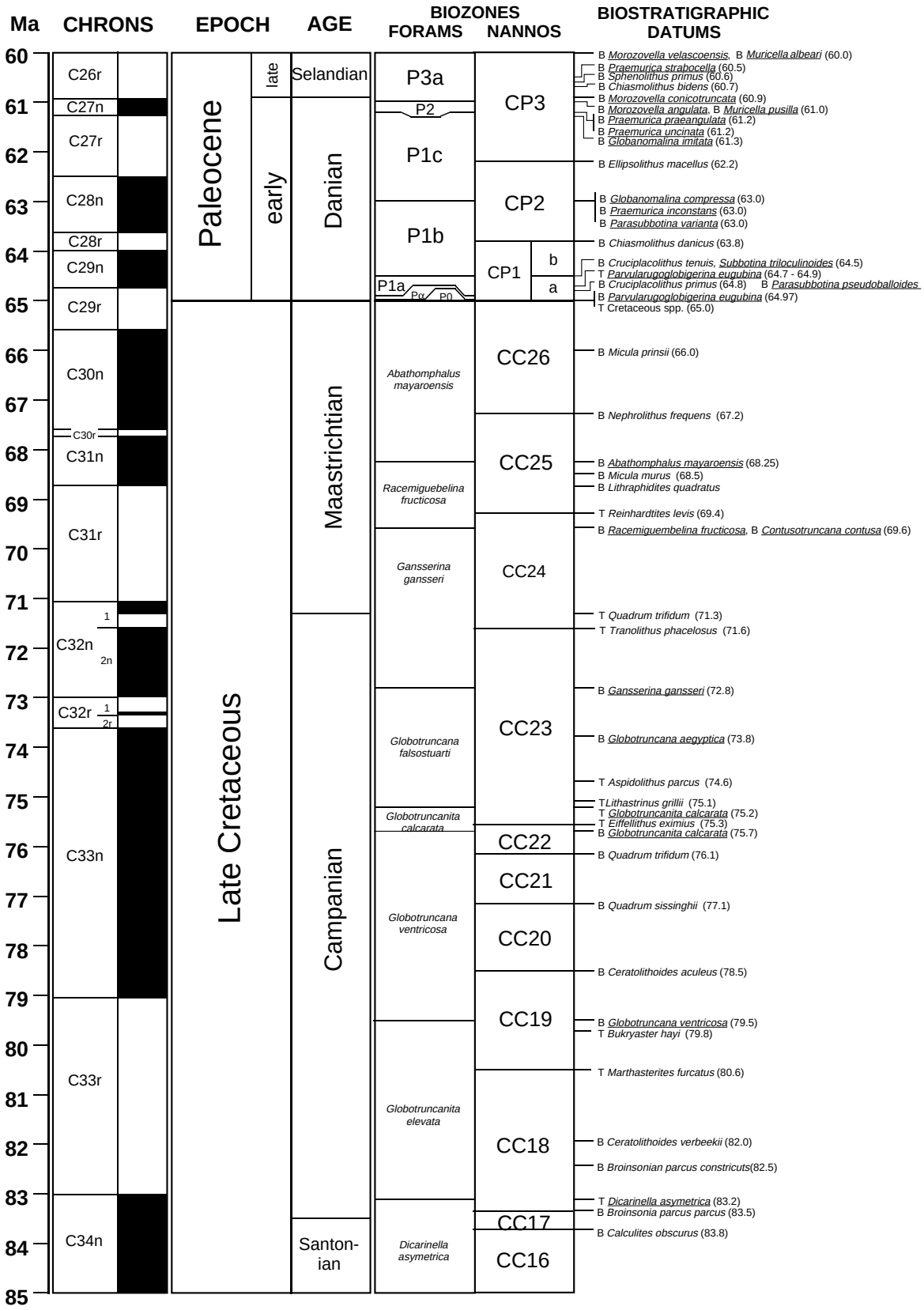

Figure 5 (continued).

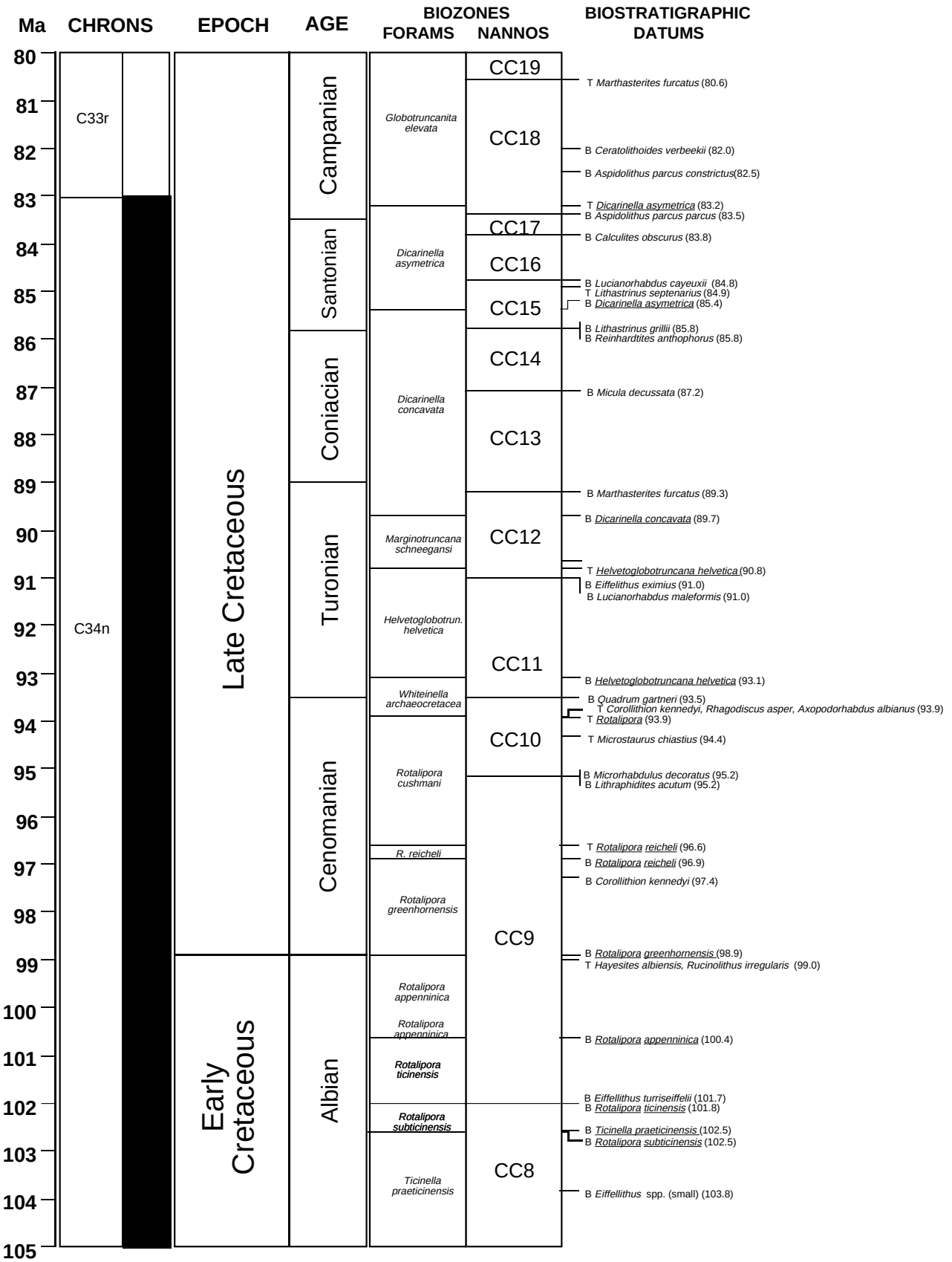

Figure 5 (continued).

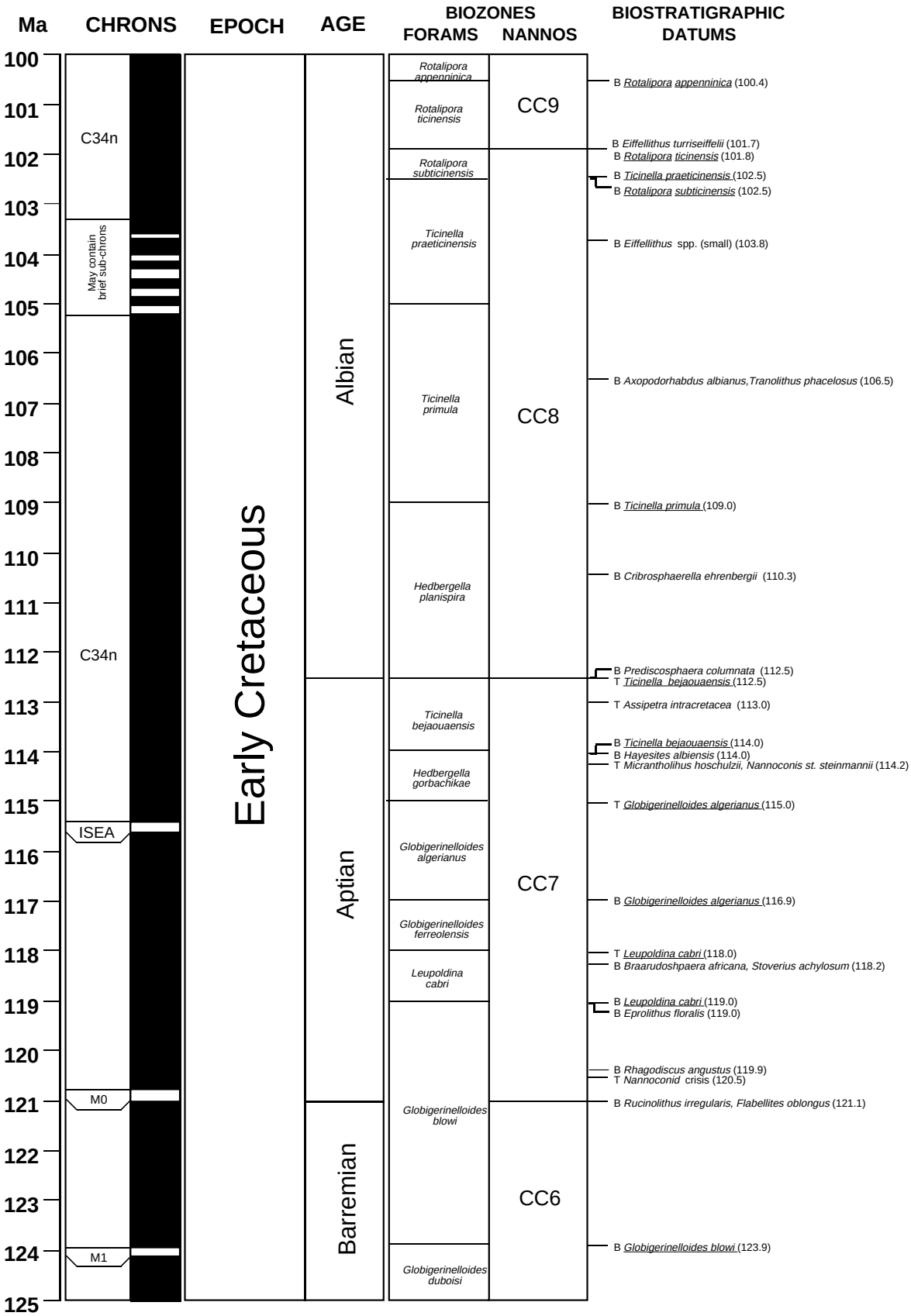

Figure 5 (continued).

Jurassic (see Fig. 6). Age estimates for most of the Cretaceous calcareous nannofossil datums were taken from Erba et al. (1995).

Calcareous Nannofossils

The zonal schemes of Martini (1971; with modifications by Martini and Müller, 1986) and Bukry (1973, 1975; zonal code numbers added and modified by Okada and Bukry, 1980) were used for Cenozoic calcareous nannofossils, whereas the zonal scheme of Sissingh (1977) as modified and/or embellished by Perch-Nielsen (1985), Applegate and Bergen (1988), Bergen (1994), and de Kaenel and Bergen (1996) was used for Cretaceous calcareous nannofossils (see Fig. 5). All of these zonations represent a general framework for the biostratigraphic classification of mid- to low-latitude floral assemblages. Age estimates for the majority of Jurassic calcareous nannofossil datums were taken from de Kaenel and Bergen (1996).

Methods

Calcareous nannofossils were examined using standard light microscope techniques, under crossed polarizers, transmitted light, and phase contrast at 1250× magnification.

Preservation and abundance of calcareous nannofossil species may vary significantly because of etching, dissolution, or calcite overgrowth. It is not uncommon to find nearly pristine specimens occurring in the same sample as specimens exhibiting overgrowth or etching. Thus, a simple code system to characterize preservation has been adopted and is listed below:

VG = very good preservation (no evidence of dissolution and/or overgrowth; no alteration of primary morphological characteristics, and specimens appear diaphanous; specimens are identifiable to the species level);

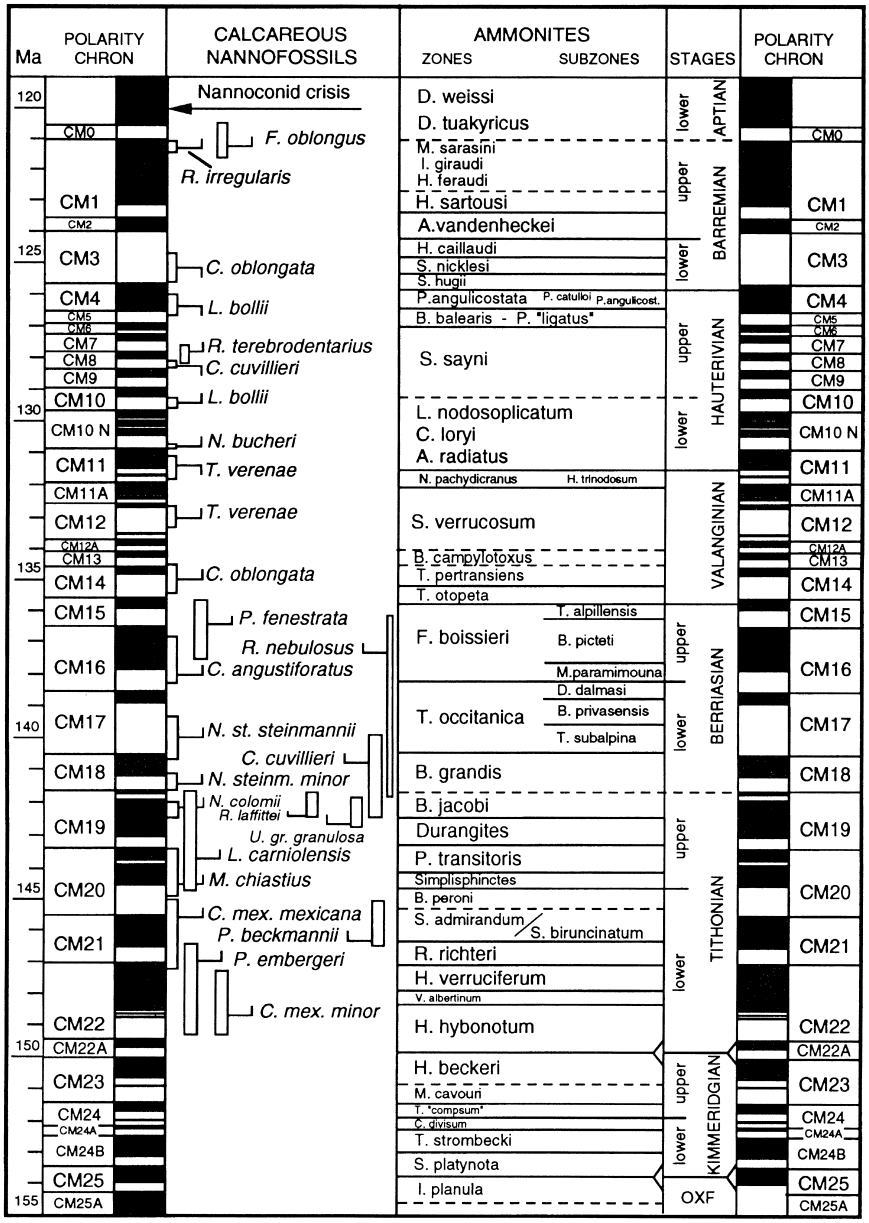

Figure 6. Early Cretaceous through Late Jurassic time scale used for this volume (from Channell et al., 1995).

G = good preservation (little or no evidence of dissolution and/or overgrowth; primary morphological characteristics only slightly altered; specimens are identifiable to the species level);
M = moderate preservation (specimens exhibit some etching and/or overgrowth; primary morphological characteristics somewhat altered; however, most specimens are identifiable to the species level); and
P = poor preservation (specimens are severely etched or exhibit overgrowth; primary morphological characteristics largely destroyed; fragmentation has occurred; specimens cannot be identified at the species and/or generic level).

Six calcareous nannofossil abundance levels are recorded as follows:

V = very abundant (10–100 specimens per field of view);
A = abundant (1–10 specimens per field of view);
C = common (1 specimen per 2–11 fields of view);
F = few (1 specimen per 11–100 fields of view);
R = rare (1 specimen per 101–1000 fields of view); and
B = barren.

Foraminifers

Methods

Foraminifers from unlithified ooze were soaked in a 10% solution of hydrogen peroxide for 20 min and then washed with tap water over a 63-µm sieve. All samples were dried on a hot plate at ~50°C and then sieved through a sieve tower of 125-, 250-, and 500-µm meshes. Species identification for planktonic foraminifers was generally made on the >250-µm and >125-µm size fractions. The 63- to 125-µm size fractions were retained in case further investigation was necessary.

The following abundance categories were estimated from visual examination of the dried sample for planktonic foraminifers:

D = dominant (>30%);
A = abundant (10%–30%);
F = few (5%–10%);
R = rare (1%–5%); and
P = present (<1%).

The following abundance categories were used for benthic foraminifer abundance at a group level, based on the number of benthic foraminifers encountered in three picking trays (where the residue volume was great enough):

A = abundant (>100 specimens);
C = common (50–100 specimens);
F = few (20–50 specimens);
R = rare (10–20 specimens); and
T = trace (<10 specimens).

The preservation status of both planktonic and benthic foraminifers is estimated as follows:

VG (very good) = no evidence of overgrowth, dissolution, or abrasion;
G (good) = little evidence of overgrowth, dissolution, or abrasion;
M (moderate) = calcite overgrowth, dissolution, or abrasion are common, but minor; and
P (poor) = substantial overgrowth, dissolution, or fragmentation.

Planktonic Foraminifer Taxonomy

Cenozoic taxonomic concepts follow Kennett and Srinivasan (1983) for the Oligocene and Miocene and Toumarkine and Luterbacher (1985) for the Paleocene and Eocene. Genus-species combinations generally follow those used by Blow (1979) and Berggren et al. (1995). Cretaceous taxonomic concepts are based on Robaszynski and Caron (1979), Robaszynski et al. (1984), and Caron (1985).

Planktonic Foraminifer Zonal Scheme and Datums

The tropical planktonic foraminifer zonal scheme for the Cenozoic and ages for the Cenozoic datums follow Berggren et al. (1995). The zonation used for Cretaceous planktonic foraminifers is based on the tropical zonal scheme of Caron (1985).

Palynology

Fourteen spot samples have been analyzed for palynomorphs in a shorebased study following the cruise. These samples comprise nine samples from Hole 1065A and five samples from Hole 1069A. Sample processing was carried out by technician Jim Davy at University College London. Analyses and interpretation of the data is the work of Susan L. Matthews, University College London, and the results are included as peer-reviewed appendices at the end of each of the relevant site chapters.

The following abundance categories were used:

A = Abundant, 20+ specimens;
C = Common, 10–19 specimens;
O = Occasional, 5–9 specimens;
R = Rare, 1–4 specimens; and
B = Barren.

IGNEOUS AND METAMORPHIC PETROLOGY

Core Curation and Shipboard Sampling

Prior to splitting igneous and metamorphic rock cores, the whole cores were examined for structural features, and unrolled digital images were taken of whole cores using the DMT Color CoreScan system (see “Core Imaging” section, this chapter). Each contiguous “piece” was then numbered sequentially from the top of each core section and labeled. Broken core fragments that could be fit together were reassembled into larger pieces; each fragment was lettered consecutively from the top down (e.g., 1A, 1B, 1C, etc.). Composite pieces sometimes occupied more than one section. Plastic spacers were placed between pieces with different numbers. If it was evident that an individual piece or fragment had not rotated about a horizontal axis during drilling, an arrow was added to the label pointing to the top of the section. The pieces were split with a diamond saw into archive and working halves. Cores were split so as to allow important features and structures to be represented in both the working and archive halves. Digital core images were also recorded on the archive half using the DMT Color CoreScan system. Images were used to aid petrological description.

The archive half was described on the visual core description (VCD) form and was photographed before storage. During this description, small samples of vein fillings, breccia matrix, altered rocks, and serpentinites were taken from the working half for XRD analysis to confirm mineral identity. Each lithostratigraphic unit or, for the breccias of Holes 1067A, 1068A, and 1070A, representative clast types were sampled in the working half of the core (where recovery

permitted) for shipboard measurement of physical properties, magnetic studies, X-ray fluorescence (XRF), and polished thin-section studies. Samples taken for thin sections were oriented (see "Structural Geology" section, this chapter). Where feasible, cubes or minicores for physical properties measurements were taken immediately adjacent to samples used for chemical analyses and polished thin sections.

Visual Core Descriptions of Igneous and Metamorphic Rocks

Visual core description forms were used in the documentation of the igneous, metamorphic, and breccia rock cores (see Section 3, this volume). The left column is a graphic representation of the archive half. A horizontal line across the entire width of the column denotes a plastic spacer. Vertically oriented pieces are indicated on the form by an arrow pointing upward to the right of the piece. Shipboard samples and studies are indicated in the column headed "shipboard studies," using the following notation:

XRD = X-ray diffraction analysis;
XRF = X-ray fluorescence analysis;
TSB = petrographic thin section;
PP = physical properties measurement; and
PM = paleomagnetic measurement.

When describing sequences of rock, the core was subdivided into basement units on the basis of texture, grain size, mineral occurrence and abundance, rock composition, and rock clast type. Rocks for which the protolith is completely obscured by metamorphism (e.g., amphibolite) were given separate lithologic names. If the original rock type is discernible, the prefix "meta" or the term "altered" is used as a modifier with the name of the protolith. Any postemplacement changes in mineralogy or structure associated with elevated temperatures or pressures were classified as "metamorphism". We reserved the term "altered" for rocks that have undergone low-temperature hydrothermal alteration or seafloor weathering. Igneous and high-temperature metamorphic minerals were termed "primary" when associated with hydrothermal alteration, and seafloor weathering minerals were termed "secondary." The following information was recorded on the visual core description forms:

1. The leg, site, hole, core number, core type, and section number.
2. The unit number (consecutive downhole, using Arabic numerals, e.g., Unit 2), position in the section, number of pieces of the same lithologic type, the rock name, and the identification of the describer.
3. The Munsell color of the wet rock surface.
4. The rock name, incorporating the most obvious mineralogical and structural characteristics of the rock (e.g., amphibolite, serpentinized peridotite, metagabbro, etc.). Igneous rock names were assigned according to essential primary minerals and/or chemical analyses following standard IUGG nomenclature (Streckeisen, 1976; Le Bas et al., 1986).
5. The texture and distribution of primary igneous and high-temperature metamorphic mineral phases visible with a hand lens. For each phase the following information was documented: (1) abundance (volume %), (2) absolute and relative sizes of crystals (in millimeters), (3) shape, (4) arrangement (e.g., layered, felted), (5) degree of alteration, and (6) further comments.
6. For plutonic rocks, the absolute ranges of grain size were recorded using the terms: very coarse-grained (crystal diameters >30 mm), coarse-grained (crystal diameters 5–30 mm), medium-grained (crystal diameters 1–5 mm), and fine-grained (crystal diameters <1 mm). Plutonic rocks were texturally classified as either equigranular, inequigranular, varitextured, or layered. Detailed descriptions were made as described in the "Explanatory Notes" chapter of the Leg 149 *Initial Reports* volume (Sawyer, Whitmarsh, Klaus, et al., 1994). Layered/cumulate textures are described following Irvine (1982).
7. For metamorphic rocks, ductile foliation (pervasive, weak, strong, mylonitic, etc.), brittle deformation (e.g., fractures, cataclasites), porphyroblasts, neoblasts, and porphyroclasts were described. Reaction textures documenting prograde and retrograde metamorphism and migmatization were also recorded.
8. For tectonic/sedimentary breccias (Sites 1067, 1068, and 1070), clasts were classified according to the criteria given above for igneous and metamorphic rocks. In addition, the maximum clast size and variations in the abundance of various clast rock types were recorded.
9. The characteristics and distribution of metamorphic, hydrothermal, and seafloor weathering minerals. Descriptors will follow those given for "5" above but will also include descriptions of veins.
10. The presence of veins and fractures, including their abundance, width, mineral fillings or coatings, orientation, and associated wall-rock alteration. The orientation of veins and fractures was measured with respect to the core reference frame (see "Structural Geology" section, this chapter). The relationship of the alteration and vein-filling minerals with respect to veins and fractures was also noted. Vein networks and their mineralogy were indicated adjacent to the graphic representation of the archive half.
11. Characteristics of (1) fault breccia, defined as any rock composed of angular broken rock fragments held together by mineral cement or a fine-grained matrix; (2) cataclasite, defined as a rock whose mineral grains or aggregates are fractured, rotated, bent, and granulated without accompanying recrystallization; and (3) mylonites, defined as a rock from a shear zone where the dominant deformation mechanism is solid-state flow and whose mineral grain sizes are often reduced in size by dynamic recrystallization.
12. Other comments, including notes on the continuity of the unit within the core and on the interrelationships of units.

Visual core descriptions of igneous and metamorphic rocks are given in Section 3 (this volume).

Thin-Section Descriptions

Thin sections were examined to complement and refine the hand-specimen observations. The same terminology was used for thin-section descriptions as was used for the megascopic descriptions. The percentages and textural descriptions of individual phases were reported. Thin-section descriptions are included in Section 6 (CD-ROM, back pocket, this volume). Tables summarizing the thin-section data are provided in each site chapter. Plagioclase determinations were performed using the Michel-Lévy method, with errors estimated as ±5 mol% An. Average values are reported in the thin-section descriptions.

X-ray Diffraction and X-ray Fluorescence Analyses

X-ray diffraction and X-ray fluorescence analyses were performed as described in the "Explanatory Notes" chapter of the Leg 149 *Initial Reports* volume (Sawyer, Whitmarsh, Klaus, et al., 1994), except that all routine shipboard samples were crushed in a tungsten carbide barrel as Nb contamination in most silicate rocks was considered to be insignificant.

Analytical conditions used during Leg 173 are given in Table 2.

Table 2. Analytical conditions used during Leg 173.

Oxide or element	Line	Crystal	Detector	Collimator	Peak angle (Å)	Background offset (Å)	Count time on peak (s)	Count time on background (s)	Detection limit
SiO_2	Kα	PET	FPC	Medium	109.21		100		0.03%
TiO_2	Kα	LIF200	FPC	Fine	86.14		100		0.01%
Al_2O_3	Kα	PET	FPC	Medium	145.12		100		0.01%
Fe_2O_3	Kα	LIF200	FPC	Fine	57.52		40		0.01%
MnO	Kα	LIF200	FPC	Fine	62.97		100		0.005%
MgO	Kα	TLAP	FPC	Medium	45.17	±0.80	150	150	0.05%
CaO	Kα	LIF200	FPC	Medium	113.09		40		0.005%
Na_2O	Kα	TLAP	FPC	Medium	54.10	–1.20	150	150	0.1%
K_2O	Kα	LIF200	FPC	Medium	136.69		100		0.005%
P_2O_5	Kα	GE111	FPC	Medium	141.04		100		0.005%
Rh	Kα-C	LIF200	Scint	Fine	18.56		100		
Nb	Kα	LIF200	Scint	Fine	21.40	+0.30	200	200	1 ppm
Zr	Kα	LIF200	Scint	Fine	22.55	–0.35	100	100	1 ppm
Y	Kα	LIF200	Scint	Fine	23.80	–0.30	100	100	1 ppm
Sr	Kα	LIF200	Scint	Fine	25.15	–0.35	100	100	1 ppm
Rb	Kα	LIF200	Scint	Fine	26.62	+0.40	100	100	1 ppm
Zn	Kα	LIF200	Scint	Fine	41.81	+0.40	100	100	2 ppm
Cu	Kα	LIF200	Scint	Fine	45.03	–0.40	100	100	2 ppm
Ni	Kα	LIF200	Scint	Fine	48.67	–0.40	100	100	2 ppm
Cr	Kα	LIF200	FPC	Fine	69.35	–0.50	100	100	3 ppm
Fe	Kα	LIF220	FPC	Fine	85.64	+0.80	100	100	
V	Kα	LIF220	FPC	Fine	123.06	–0.50	100	100	4 ppm
Ti	Kα	LIF200	FPC	Fine	86.14	–0.50	100	100	
Ce	Lα	LIF220	FPC	Medium	128.16	+1.89	100	100	10 ppm
Ba	Lβ	LIF220	FPC	Medium	128.78	+1.31	100	100	15 ppm

Notes: Analyses were performed using a rhodium-target X-ray tube operated at 30 kV and 80 mA for major elements and 50 kV and 50 mA for trace elements. Detectors: FPC = flow proportional counter (P_{10} gas); Scint = NaI scintillation counter. Elements Rh, Fe, and Ti were measured by the trace element program for matrix and interference corrections only.

STRUCTURAL GEOLOGY

Introduction

The structural studies performed on the cores from Leg 173 were designed to (1) document all deformation structures and their relative ages (overprinting relations), (2) establish the probable range of temperature conditions under which individual structures formed, (3) establish the orientation and, if possible, kinematics (shear sense) of faults and shear zones, (4) determine the probable tectono-sedimentary history of breccia zones, and (5) assess the role of fluids in deformation processes.

The methods used here were designed following the "Explanatory Notes" chapters of the *Initial Reports* volumes for earlier ODP Legs, mainly Legs 131 (Taira, Hill, Firth, et al., 1991), 149 (Sawyer, Whitmarsh, Klaus, et al., 1994), 153 (Cannat, Carson, Miller, et al., 1995), and 159 (Mascle, Lohmann, Clift, et al., 1996). Modifications were made where they seemed appropriate in order to meet the specific needs and problems of Leg 173.

An important consideration is that commonly only part of the cored interval associated with any one core is actually recovered, leading to a sampling bias that for structural purposes is particularly acute. In particular, in cases of incomplete recovery, material from fault zones may be missing. When faulted or fractured rock from such zones is recovered, it is often highly disturbed and its original orientation has changed.

Graphical Representation and Terminology

The structures on the core face of the archive half were drawn on Structural Geology Description forms. These can be found in Section 3. Information on specific structures was recorded on the Structural Log Sheets. In addition, two columns, one for a simplified graphical representation of the most important structures and one for measurements and identifications of structures, were added to the Visual Core Description (VCD) forms. The descriptive terminology we used for macroscopic features in hard rocks is listed in Figure 7. Those terms that are not specified in the comments column of Figure 7 were used following Ramsay and Huber (1983, 1987).

Overprinting relations between structures were expressed in the VCD forms by linking identifiers with hyphens. For example, "B-V-S" means that a foliation (S) is overprinted by veins (V) and then brecciated (B).

Structural Measurements

Determining the orientation of observed structures (and intrusive dikes) in the geographical reference frame is difficult. Therefore, structures were first oriented with respect to the core reference frame. Where possible, this arbitrary reference frame was related to true north and true vertical using paleomagnetic data partly supplemented with images provided by the DMT core scanner (see below). The core reference frame was chosen according to the ODP magnetic direction conventions to allow direct comparison with the paleomagnetic results (Fig. 8). The plane perpendicular to the long axis of the core was taken as the horizontal. "North," "south," "east," and "west" were defined in this plane in the following manner: south (azimuth 180°) is the direction perpendicular to the cut surface of the archive-half pointing toward the cylindrical outer surface of the archive half. Consequently, north (azimuth 000°) is the opposite direction, pointing into the working half. With the archive half oriented top-up, west (270°) is directed toward the right side of the surface of the archive half, east (090°) toward the left side.

The orientations of linear and planar elements were documented using dip azimuth and dip angle. The orientation is always expressed by two numbers of which the first indicates the dip azimuth and the second the dip angle (e.g., 090/45 means a plane or a line dipping or plunging "east" at an angle of 45°). Our measurements of the orientations of planar structures observed in the cores were greatly facilitated by a simple tool described in the "Explanatory Notes" chapter of the Leg 131 *Initial Reports* volume (Taira, Hill, Firth, et al., 1991). For planar elements, the apparent dip on the core face was measured, either dipping toward the "east" or toward the "west." The orientation of the planar element was then completely constrained using an additional measurement either from the horizontal plane (top or bottom of piece) or from the cylindrical outer surface of the core half, as shown in Figure 12 of the "Explanatory Notes" chapter of Taira, Hill, Firth, et al. (1991). The two measurements yielded the orientations of two

Tectonic feature identifiers

Identifier	ID	Comments
Planar features		
primary layering	PL	Compositional layering; e.g., in ultramafics, marked by layers of pyroxenite in peridotite
bedding	So	
foliation	S	Defined by preferred orientation of unequant minerals or mineral aggregates
high-T foliation	S_{HT}	Main mineral constituents underwent crystal plastic deformation
low-T foliation	S_{LT}	Brittle deformation prevailing (e.g., in foliated cataclasite)
relict foliation	rS	
C surface	C	Shear surface in an S-C fabric
shear band	C'	
slaty cleavage	CL	
crenulation cleavage	CC	
fault	X	Discrete surface with visible offset
joint	J	Discrete surface without any visible offset
vein	V	Subscripts: c=calcite; q=quartz; fsp=feldspar; ch=chlorite; ep=epidote; serp=serpentine; Fe=Fe-oxide; tc=talc; pyr=pyrite; li=limonite; pr=prehnite; chal=chalcedony
open vein	Vo	
magmatic vein	V_{mg}	
sheared vein	XV	
dike	D	
igneous contact	I	
Deformation zones		
mylonite zone	M	
cataclasite zone	CT	
breccia zone	B	
microbreccia zone	µB	
crackle breccia zone	cB	Original clast can be pieced together from "jigsaw" fragments
fault gouge	XG	
Linear features		
stretching lineation	L_{ST}	Defined by preferred orientation of elongated minerals or mineral aggregates
slickenside lineation	L_{SL}	Mechanically produced small grooves and ridges
slickenfibre lineation	L_{SF}	Lineation on fault surface formed by newly grown fibrous minerals
Folds	F	
slumps	F_S	In soft sediments
kinks	F_K	
fold axial plane	F_{AP}	
fold axis	FA	
Other features		
porphyroclasts	P	
fragment or clast	Fr	
Shear-sense indicators	Y	
drag	Y_D	
s-c fabric, shear bands	Y_C	
porphyroclasts	Y_P	

Figure 7. Terminology used for structural description during Leg 173.

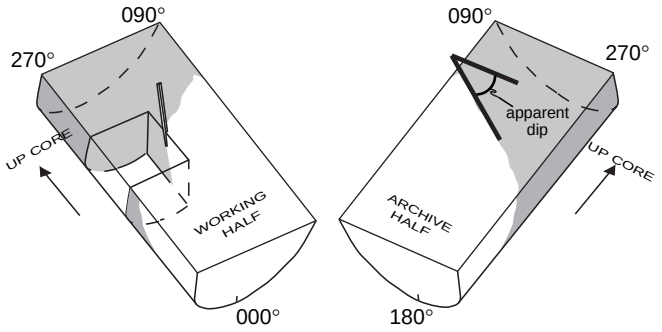

Figure 8. Core reference frame used during Leg 173.

lines contained within the planar element. The orientation of the planar element itself was then determined from the orientation of the two lines using a stereonet. This procedure provided the working azimuth and dip of the observed structure (i.e., the azimuth and dip within the core reference frame). The dip is "true," as long as the core axis is approximately vertical. The orientations of linear structures were recorded as "working trends." These were measured using dip azimuth and dip angle and referred to the core reference frame in the same way as planar surfaces.

In some cases, where uniformly dipping sediments were cored, just the core liner was split and the recovered material was reoriented before cutting the core, to remove the relative vertical-axis rotations of individual pieces induced by rotary coring. The pieces were reoriented in such a way that the dip azimuth of bedding was always toward the east in the core reference frame. This allowed for much more rapid and accurate measurement of the true dips of bedding and proved to be useful also for the pass-through magnetometer measurements, which gave more consistent declinations.

The sense of fault displacement was recorded and referred to as normal, reverse, sinistral strike-slip, or dextral strike-slip. The apparent displacement was measured on the core face and/or on the top or bottom side of pieces. In cases where the direction of slip was visible, offset was measured in a plane normal to the fault and parallel to this direction, as straight-line separation between displaced markers. Mineral and/or mylonitic foliations and lineations were measured in much the same way as faults and veins. If the cut surfaces were chosen to be parallel to lineations and perpendicular to foliations, they could be measured directly.

Geographic Orientation of Structures

At this stage, the structures were oriented in the core reference frame, although not with respect to geographical ordinates. Reorientation was next attempted using paleomagnetic data partly in combination with core scanning.

Paleomagnetic measurements were made on the core (see "Paleomagnetism" section, this chapter) using a pass-through cryogenic magnetometer and on discrete samples taken from the core. In some cases, a component of viscous remanent magnetization (VRM) was determined by demagnetization of discrete samples. Because this component is known usually to parallel the present-day magnetic field, it can be used to reorient structural features. To reorient these features in the geographic reference frame, the amount of declination of the VRM is subtracted from the azimuth of the structural feature measured in the core reference frame, which corresponds to a vertical-axis rotation. This latter method proved to be useful for orienting both bedding in sediments (see "Structural Geology" section, "Site 1067" chapter, this volume) and veins and foliations in basement rocks (see "Structural Geology" section, "Site 1068" section, this volume). In one case, the stable components of the magnetization of several pieces of metasedimentary rock could be used to decide whether these pieces belonged to continuous basement or had been resedimented (see "Structural Geology" section, "Site 1069" chapter, this volume).

It was intended to use logging tools such as the Formation MicroScanner (FMS) to reorient the core. However, hole collapse and equipment failure inhibited successful FMS logging, which was only achieved at Site 1065 during Leg 173. Reorientation of the core may be obtained by correlation of unrolled DMT core scanner images and FMS images, as the FMS contains three fluxgate magnetometers (see "Core Imaging" section, this chapter). The difference between the diameter of the borehole and that of the core causes difficulty in correlating features. Hence, such a correlation would be more successful for orientation purposes for individual features such as a single well-marked joint, a well-developed foliation, or a layering pattern that can be recognized on both downhole images and on the core. FMS data, when compared with paleomagnetic measurements, would also potentially allow identification of tectonic rotations of the magnetization vector.

Thin-Section Description

Thin sections of basement rocks recovered during Leg 173 were examined in order to (1) confirm macroscopic descriptions of ductile and brittle structures, (2) characterize the microstructure of the rocks, (3) provide information on the kinematics of ductile and brittle deformation, (4) assess the role of fluid in contributing to deformation, and (5) document major structural zones and downhole variations. For the description of microstructures we applied the terminology of Passchier and Trouw (1996). Shipboard thin sections were generally oriented, except when they were made from small pieces whose orientation with respect to the rest of the core was unknown. The orientation referred to the core reference frame and was marked on each thin section by an arrow pointing upward and a short tick pointing toward "west" from the base of the arrow. Marking two directions is necessary in order to achieve complete orientation of thin sections cut parallel to the cut surface of the core.

CORE IMAGING

General Objectives

The principal objectives of the core imaging program were closely connected to the main scientific goals of this cruise. They can be identified as follows:

1. Provision of a comprehensive set of digital core images, including both unrolled 360° and slabbed images, recorded using the DMT Color CoreScan system (see below);
2. Identification and measurement of planar features on unrolled images for comparison with core structural analysis (see "Structural Geology" section, this chapter) and integration with geographically oriented FMS images (see "Downhole Measurements" section, this chapter);
3. Depth matching and reorientation to true geographic north of core and structural data obtained from the General Purpose Inclinometer Tool of the FMS; and
4. Calculation of lithological diversity using digital analysis of slabbed core images.

DMT Color CoreScan System

The DMT Color CoreScan system is a stand-alone portable core-imaging unit (Fig. 9). Images are recorded in both slabbed and un-

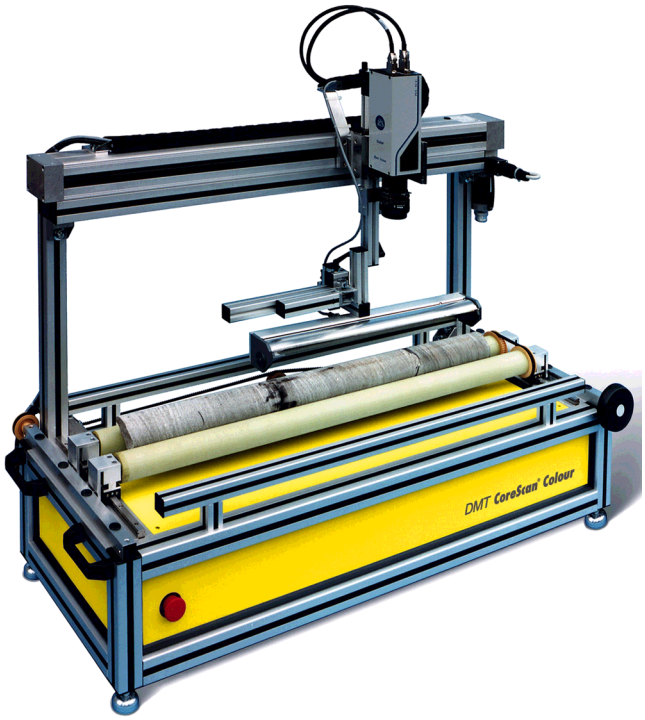

Figure 9. The DMT Color CoreScan System, showing scanning of a whole core.

rolled modes using a 24-bit, three-color (red, green, blue) CCD line scan camera with a resolution of 5184 pixels per meter (131 pixels per inch) and spectral response of between 400 and 700 nm. A more detailed description of the DMT CoreScan can be found in Weber (1994). In the unrolled mode, whole-round core is rotated around its cylindrical axis with the camera line scan positioned parallel to the axis of rotation. Unrolled images up to a length of 1 m are recorded in 33-cm sections that are integrated and light calibrated using the DMTGrab Software (DMT-GeoTec/Geo-Engineering, 1996). In the unrolled mode 1-m-long whole-round cores are scanned in ~1.20 min and create a 14-MB bitmap file.

Split archive-half core images up to 1 m long are recorded with the camera line scan traveling perpendicular to the vertical core axis. Scanning 1 m of split core takes ~45 s and creates a 5-MB bitmap file.

Imaging Strategy

Unrolled images of consolidated sedimentary and basement material were recorded after the core had been run through the multisensor track (MST) and before splitting. A vertical line scribed on the core aided initial reorientation of images back to the ODP reference frame (see "Paleomagnetism" and "Structural Geology" sections, this chapter). Unrolled images consisted of contiguous core pieces whenever possible. The lengths of whole-round pieces unsuitable for scanning were measured so allowances could be made for them when images were integrated into core barrel lengths, using the DMT Software CoreLog (DMT-GeoTec/Geo-Engineering, 1996). Initial structural analysis was carried out on board; however, the majority of the structural analysis and core reorientation work will be carried out postcruise.

Split core images were made of both sedimentary and basement archive-half cores after VCDs had been made. Comparisons of bedding planes measured on sedimentary cores were made using digital image analysis. Binary images were made of whole-core images using the public domain NIH Image program where clearly identifiable

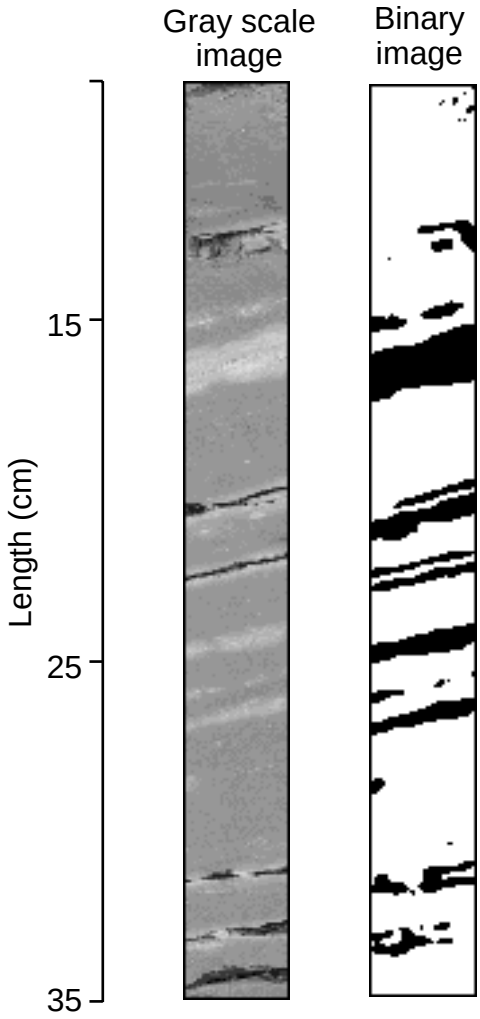

Figure 10. Example of gray scale and binary images (interval 173-1067A-10R-1, 8–35 cm), showing a sequence of alternating colored beds used for automated dip analysis.

sequences of beds with alternating colors could be seen. This allowed the creation of black-and-white binary images of the alternating colored divisions (Fig. 10). Apparent dips of the beds (black) were then calculated by computing the angle between the horizontal and the long axis of an ellipse fitted to the bedding layer (see NIH Image 1.58 Manual, 1997, for procedure). Bedding dips measured on the images were then compared with bedding dips measured directly from the cores. Similar binary image analysis techniques were used to identify breccia–clast/matrix variations and the modal mineralogy of basement rocks. Postcruise digital image analysis of the split core surface will use a variety of techniques to identify and quantify lithological diversity, modal mineralogy, and the density and geometry of structural features and their relationship in time and space.

PALEOMAGNETISM

Paleomagnetic studies conducted on board the *JOIDES Resolution* during Leg 173 consisted of routine measurements of natural remanent magnetization (NRM) and of magnetic susceptibility of sedimentary and basement material. Remanent magnetization measurements conducted on the archive-half of core sections (up to 1.5 m

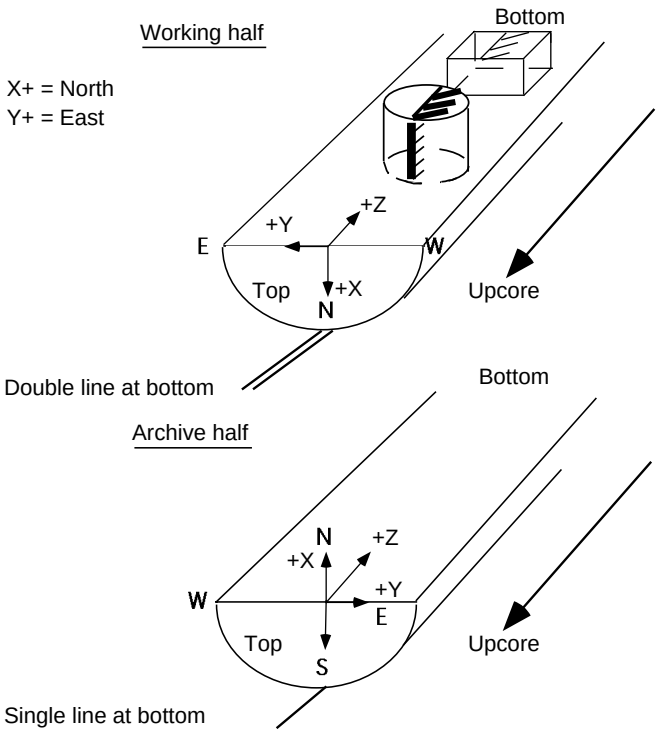

Figure 11. The ODP core orientation scheme arbitrarily designates the positive X-axis direction as the horizontal ("north") direction from the center of the core to the median line between a pair of lines inscribed lengthwise on the working-half of each core liner. Correspondingly, the negative X-axis direction ("south") is the horizontal direction from the center of the core to a single line inscribed lengthwise on the archive-half of each core liner.

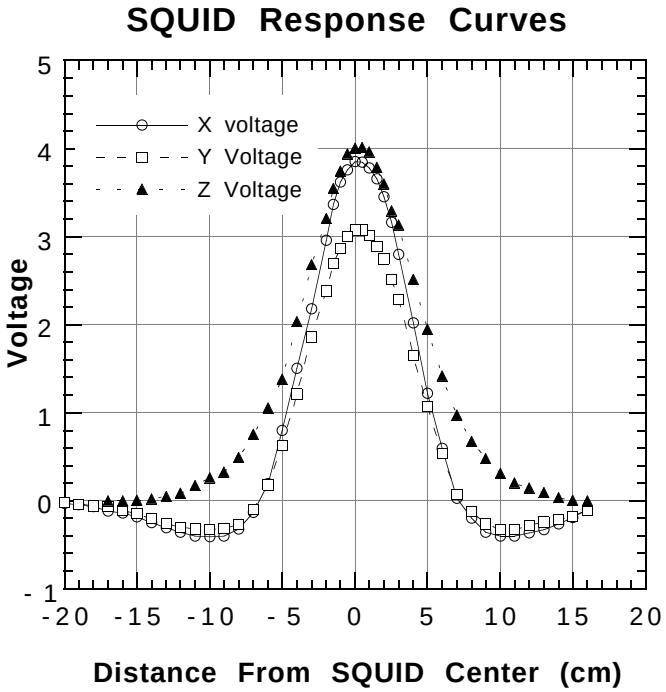

Figure 12. The response curves of the cryogenic superconducting DC-SQUID magnetometer (2-G Enterprises Model 760-R).

long) and discrete minicore samples (2.54 cm diameter by 2.54 cm long) collected from the working-half sections were performed using an automated pass-through cryogenic superconducting DC-SQUID rock magnetometer (2-G Enterprises Model 760-R) with an in-line alternating field (AF) demagnetizer, capable of reaching peak fields of 80 mT (2-G Enterprises Model 2G600). Magnetic susceptibility was measured for whole-core sections using a Bartington Instruments magnetic susceptibility meter (model MS2C) with an 88-mm-diameter whole-core sensor loop set at 0.565-kHz frequency. The magnetic susceptibility values are not volume corrected (see "Physical Properties" section, this chapter, for unit conversions and volume corrections). The susceptibility meter is part of the multisensor track (MST), which also contains a gamma-ray attenuation porosity evaluator (GRAPE) and compressional-wave logger (see "Physical Properties" section, this chapter). Susceptibilities of discrete samples were measured on a second Bartington Instruments magnetic susceptibility meter (model MS2C). Most discrete samples were stepwise thermally demagnetized using the Schonstedt thermal specimen demagnetizer (Model TSD-1). The magnetic susceptibility of the samples was monitored between each temperature step as a means of assessing any irreversible mineralogical changes associated with heating. All discrete sample susceptibilities have been corrected for the calculated cylindrical sample volume.

Postcruise, an error was found in the cryogenic magnetometer software that affects the declination values. All of the data files in the ODP database have been corrected for this error by multiplying the Y-axis component of the magnetic moment and intensity by –1.

Similarly, the raw declination values are corrected by multiplying by –1. For example, an uncorrected declination of 330° becomes 30° (360° – 330° = 30°). Again, this correction does not affect the inclination or total field intensity. It will be noted in the tables and figures of this report whether the correction has been made.

Remanent Magnetization Measurements

The ODP core orientation scheme arbitrarily designates the positive X-axis direction as the horizontal ("north" in the structural geologists' reference frame) direction from the center of the core to the median line between a pair of lines inscribed lengthwise on the working half of each core liner (Fig. 11). The NRM and remanence measurements after progressive AF demagnetization were routinely measured at 5-cm intervals. Progressive AF demagnetization steps, incremented by 10 mT, were typically at 10, 20, 30, 40, 50, and 60 mT. When the cryogenic magnetometer makes continuous measurements, it assumes a uniformly magnetized core; this provides the most reliable directional data, so long as the core being measured is longer than the sensing region. Tests conducted during previous legs (e.g., Leg 131) indicate that in cases where the core is not uniformly magnetized, either through natural processes or artifacts (voids in the core or differential rotation of segments within the core liner [biscuiting]), the values of declination, inclination, and intensity need careful evaluation. For this reason, at least one discrete shipboard paleomagnetic sample was taken from each section and from each representative lithology for progressive AF and/or thermal demagnetization to characterize the magnetic behavior. The response curves of the cryogenic magnetometer (Fig. 12) allow for rapid demagnetization and measurement of seven discrete samples per pass-through.

Sampling

Discrete samples of soft sediment were taken using oriented standard plastic boxes (6 cm^3), with an arrow pointing in the uphole direction (Fig. 11). In order to reduce the deformation of the sediment, the core was cut using a thin stainless steel spatula before pressing the plastic boxes into the sediment. Minicores (10 cm^3) were drilled from lithified sedimentary and crystalline rocks using a water-cooled non-

magnetic drill bit attached to a standard drill press. Minicores were oriented in a similar manner, with an arrow pointing in the uphole direction (Fig. 11). Discrete samples used in pilot demagnetization studies were typically taken at an increment of one per section. However, discrete samples were taken at smaller increments (as small as every 10 cm) to examine geomagnetic reversals, key geologic boundaries, or other intervals of interest.

Perturbations by Drilling and Spurious Magnetization

In addition to the mechanical disturbance of unconsolidated sediments that can occur during rotary coring, which complicates the interpretation of measurements made by the pass-through cryogenic magnetometer, another persistent problem is the pervasive remagnetization associated with drilling. As noted on previous legs, samples are exposed to large magnetic fields on the rig floor (Keating, 1984) and may be contaminated by rust (observed during Leg 115; Shipboard Scientific Party, 1988), and these two effects have been suggested as sources of these remagnetizations. In addition, previous studies of discrete samples taken from the center of the working-half section tended to show shallower inclination; indicating that the intensity of the overprint decreases radially from the edge to the center of the core (observed during Leg 134; Shipboard Scientific Party, 1992), suggesting that the core barrel is the most significant source of this overprint. At all sites, low-coercivity sediments and rocks showed strong NRM intensities and steep positive inclinations, 70° or greater. This steep inclination is subparallel to the axis of the drill string and core barrel. Isolation of the primary component of magnetization in the discrete samples generally required AF demagnetization of 15 to 25 mT (Fig. 13). Thus, this drilling-induced remagnetization can be considered as a viscous remanence or may be comparable to a strong field (>20 mT) isothermal remanent magnetization.

During demagnetization of the discrete samples with the in-line AF demagnetizer, several samples acquired spurious magnetizations above 40 to 50 mT. These spurious magnetizations typically appear as a tightening spiral on a vector component diagram (Fig. 13). During the leg the software that ran the cryogenic magnetometer and the inline AF demagnetizer demagnetized samples using the following sequence; X, Y, and Z. This sequence was repeated for each AF demagnetization step. The spurious magnetizations are most likely to be the sum of two types: an anhysteretic remanence produced along the axis of demagnetization and a sample-dependent component of gyromagnetic origin that was produced mostly orthogonal to the axis of demagnetization. This could be tested by measurements after demagnetization along each positive and negative axis and corrected by randomly changing the AF demagnetization sequences in the long-core magnetometer program.

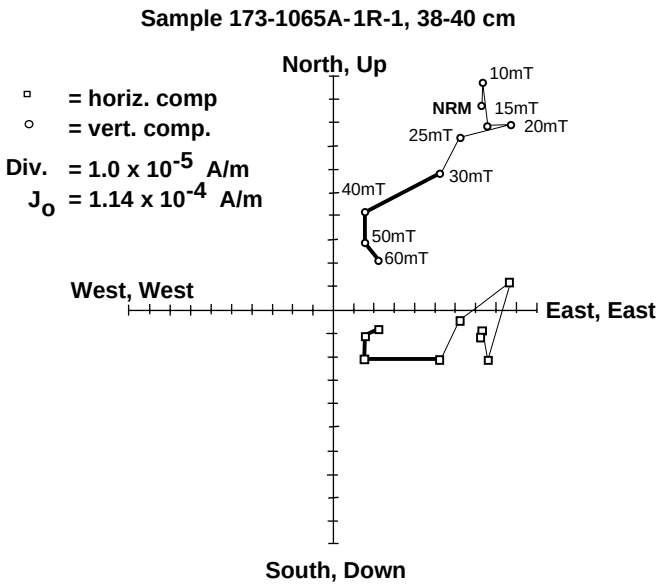

Figure 13. During demagnetization of the discrete samples with the in-line alternating field demagnetizer (2-G Enterprises Model 2G600), samples acquired spurious magnetizations above 40 to 50 mT. These spurious magnetizations typically appear as a tightening spiral on a vector component diagram, as indicated by bold lines connecting the 30 through 60 mT steps in an example of such measurements made on Sample 173-1065A-1R-1, 38–40 cm. J_o is the initial magnetic intensity. (Note: The declinations have not been corrected in this figure; see "Paleomagnetism" section, this chapter).

Magnetostratigraphy and Application of Viscous Remanent Magnetization

Where magnetic cleaning successfully isolated the primary component of remanence, paleomagnetic inclinations are used to assign a magnetic polarity to the stratigraphic column. Interpretations of the magnetic polarity stratigraphy, constrained by biostratigraphic data, are presented in the site chapters. The revised time scale of Berggren et al. (1995) was used for the Cenozoic polarity boundaries. The time scale of Gradstein et al. (1995) was used for Mesozoic rocks and sediments.

As mentioned above, discrete paleomagnetic samples taken from the center of the working-half section are less affected by drilling-induced remagnetization. For these samples, the secondary (soft) components of magnetization removed during initial stages of thermal and AF demagnetization are mainly VRM in origin. Natural VRM is gradually acquired during exposure to weak magnetic fields, such as Earth's, and is thus an undesirable noise from the paleomagnetic point of view. Because of logarithmic growth of VRM with time of exposure, however, VRM is dominated by the most recent magnetic field and is usually observed to have aligned with the present geomagnetic field. Therefore, VRM can be useful in reorienting ODP cores and structures within cores. During Leg 173, we specifically targeted several cores that were not disturbed by drilling and contained well-developed foliation for the application of the VRM components. Because the inclinations of the soft component from these core samples were similar to that of the present-day field at Leg 173 drill sites, we speculate that the soft component is either a viscous magnetization or was recently acquired during alteration. Based on this assumption, the VRM represents the direction of the present geomagnetic field and can be applied to reorient the core sections in the geographic reference frame. This hypothesis may be tested by using available corresponding images from the FMS and attitudes of the foliation planes that correlate well with the tectonic/structural setting of the region.

Magnetic Susceptibility Measurements and the Königsberger Ratio

Susceptibility measurements made on the whole core following the establishment of the final curated positions and placement of spacers are directly comparable with the pass-through measurements of archive-half cores. The general trend of the susceptibility data curve was used to characterize the magnetic material contained within the cored material. The susceptibility response is a function of the mineralogy as well as the shape and volume of the magnetic particles within the rocks. Susceptibility provides an indication of the amount of magnetic material in the core and was used to consider locations for taking discrete samples for further paleomagnetic measurements.

The volume susceptibility was used in conjunction with the NRM intensity to calculate the Königsberger ratio (Q, the ratio of remanent

to induced magnetization) of the samples. The International Geomagnetic Reference field (IGRF) value at the Leg 173 sites (45,000 nT = 35.83 A/m) was used for calculating Q (Q = NRM [A/m] /{*k* [SI] × *H* [A/m]}), where *H* is the local geomagnetic field and *k* is the susceptibility. In general, the Königsberger ratio is used as a measure of stability to indicate a rock's capability of maintaining a stable remanence. Among the Leg 173 sites, the Königsberger ratio is a useful parameter in evaluating the contribution of the effective magnetization resulting from the susceptibility of the rocks to the regional magnetic anomalies, as the Königsberger ratio is a linear function of NRM/induced magnetization.

ORGANIC AND INORGANIC GEOCHEMISTRY

Shipboard interstitial water analyses were performed on water squeezed from 5- to 10-cm-long whole-round sediment samples using Manheim squeezers (Manheim and Sayles, 1974). Salinity, alkalinity, and pH were analyzed according to methods described in Gieskes et al. (1991). Calcium and magnesium were analyzed by ion chromatography using a Dionex DX-100 ion chromatograph. The precision of the analyses is comparable to those given in recent *Initial Reports* volumes (e.g., ODP Leg 164; Shipboard Scientific Party, 1996).

The shipboard organic geochemistry program included (1) monitoring of hydrocarbon gases, (2) measurement of sedimentary inorganic (carbonate) carbon, and (3) elemental analysis of total carbon, total nitrogen, and total sulfur. Standard ODP methods and instruments for sample collection and analyses were used as described by Kvenvolden and McDonald (1986) and in the "Explanatory Notes" chapters of the *Initial Reports* volumes for recent legs (e.g., Leg 164; Shipboard Scientific Party, 1996). The composition and concentration of hydrocarbons and other gases, sampled from the sediments using the headspace method, were analyzed at an interval of once per core.

PHYSICAL PROPERTIES

Introduction

Shipboard physical properties measurements provide a first look at variations in core characteristics and may be correlated with downhole measurements, regional seismic studies, visual core descriptions, and related fabric studies. Physical properties data offer the possibility of defining the deformation state of sediments and rocks, thereby contributing to one of the principal objectives of Leg 173.

Nondestructive measurements were made on whole sections of core using the MST. The MST included the GRAPE, compressional-wave logger (PWL), magnetic susceptibility meter (MSM), and a natural gamma radiation (NGR) sensor. Thermal conductivity measurements were also made on sediments and basement rocks using the needle probe method. If the sediment was soft enough, compressional-wave velocities were measured on the working half of the core. In addition, discrete samples were taken throughout the cores to determine of index properties and compressional-wave velocities.

Nondestructive Measurements

Multisensor Track

The GRAPE measures bulk density at 1-cm intervals (minimum) by comparing the attenuation of gamma rays through the cores with attenuation through aluminum and water standards (Boyce, 1976). GRAPE data are most reliable in undisturbed cores and offer the potential of direct correlation with downhole bulk density logs. For discontinuous, fragmented core that did not completely fill the core liner, GRAPE acquisition was turned off.

The PWL transmits a 500-kHz compressional-wave pulse through the core. The transmitting and receiving transducers are aligned perpendicular to the long axis of the core (Z-direction). A pair of displacement transducers monitors the separation between the compressional-wave transducers. Measurements are taken at 3-cm intervals. As with the GRAPE sensor, only continuous cores that filled their core liners were measured. The quality of the data was assessed by examining the arrival time and amplitude of the received pulse. Data with anomalously large travel times or low amplitudes were discarded.

Magnetic susceptibility was measured on all sections at 3- to 5-cm intervals using the 1.0 (1 s integration time) range on the Bartington meter (model MS2C), which has an 8.8-cm diameter loop. The meter was set on SI units, and the values were stored in the JANUS database in raw meter units. In our discussions of the data, we convert to SI units by multiplying by 10^{-5}. A further correction factor of 0.66, to account for full core volumes, was not applied because core liners were often not full. Magnetic susceptibility aids the detection of fine variations in magnetic intensity associated with magnetic reversals or lithologic changes. The quality of these results is degraded in rotary core barrel (RCB) sections if the core liner is not completely filled and/or the core is disturbed. However, general downhole trends may still be used for laboratory-to-well-log correlation.

Natural gamma-ray emission was measured at 30-cm intervals in each section. The length of influence for the four NGR sensors is about ±10 cm from their points of measurement along the core. The installation and operating procedures for the NGR system used during Leg 173 are discussed by Hoppie et al. (1994). Data from 2048 energy channels were collected and archived. Counts were summed over a range (200–3000 keV) to be comparable to data collected on previous legs. This integration range also allows for direct comparison with downhole logging data. Over the 200–3000 keV integration range, background counts measured using a core liner filled with distilled water averaged 18 per 30-s measurement period. No corrections were made to NGR measurements made on extended core barrel (XCB) or RCB cores to account for sediment incompletely filling the core liner. Before starting measurements, the four sensor gains were adjusted so that the combined potassium peak was as sharp as the individual peaks when the other three sensors were disabled. The multichannel analyzer was calibrated by assigning certain channels to the characteristic energies of ^{40}K and the main peak of ^{232}Th (Ocean Drilling Program, 1996).

Thermal Conductivity

Whole-round core sections were allowed to adjust to room temperature for at least 2 hr in preparation for thermal conductivity measurements. The needle probe method was used in full-space configuration for soft sediments (Von Herzen and Maxwell, 1959), and in half-space mode (Vacquier, 1985) for lithified sediment and hard rock samples. Measurements were typically made in every other section.

Soft Sediment "Full-Space" Measurements

A needle probe containing a heater wire and a calibrated thermistor was inserted into the sediment through a small hole drilled in the core liner before the sections were split. The probe was positioned where the sample appeared to show uniform properties. Measurements were taken using a single-probe TeKa (Berlin) TK-04 unit.

At the beginning of each measurement, temperatures in the samples were monitored without applying current to the heating element to verify that temperature drift was less than 0.04°C/min. The heater was then turned on, and the temperature rise in the probes was recorded. After heating for about 60 s, the needle probe behaves approximately as a line source with constant heat generation per unit length. Temperatures recorded between 60 and 240 s were fit to the follow-

ing equation using the least-squares method (von Herzen and Maxwell, 1959):

$$T(t) = (q/4\pi k)\cdot\ln(t) + L(t), \quad (1)$$

where k is the apparent thermal conductivity (W/[m·K]), T is temperature (°C), t is time (s), and q is the heat input per unit length of wire (W/m). The term $L(t)$ corrects for temperature drift, described by the following equation:

$$L(t) = A\,t + T_e, \quad (2)$$

where A represents the rate of temperature change, and T_e is the equilibrium temperature.

Lithified Sediment and Hard Rock "Half-Space" Measurements

Half-space measurements were made on selected lithified sediments and crystalline rock samples after the cores had been split and their faces polished. The needle probe rested between the polished surface and a grooved epoxy block with relatively low conductivity (Sass et al., 1984; Vacquier, 1985). Half-space measurements were conducted in a water bath to keep the samples saturated, to improve the thermal contact between the needle and the sample, and to reduce thermal drift. EG&G thermal joint compound was also used to improve the thermal contact. Data collection and reduction procedures for half-space tests are similar to those for full-space tests except for a multiplicative constant of 0.5 in Equation 2, which accounts for the different experimental geometry.

Discrete Measurements

Index Properties

Samples of approximately 10 cm^3 were taken for determination of index properties. Bulk density, grain density, water content, porosity, and dry density were calculated from wet and dry sample weights and dry volumes.

Sample mass was determined to a precision of ±0.001 g using a Scitech electronic balance. The balance was equipped with a computer averaging system that corrected for ship accelerations. Sample volumes were determined using a Quantachrome Penta-Pycnometer, which is a helium-displacement pycnometer with a nominal precision of ±0.02 cm^3 but apparently with a lower experimental precision (±0.04 cm^3). Sample volumes were measured at least three times, until readings were consistent. A standard reference volume was run with each group of samples during all the measurements to determine instrument drift.

Water Content

The determination of water content as a fraction of total mass or as a ratio of water mass to solid mass followed the methods of the American Society for Testing and Materials (ASTM) designation (D) 2216 (ASTM, 1989). Total mass (M_t) and dry mass (M_d) were measured using the electronic balance and the difference was taken as the uncorrected water mass. Measurements were corrected for salt assuming a pore-water salinity (r) of 0.035, following the discussion by Boyce (1976). The equations for the two water-content calculations are:

$$W_d\,(\%\text{ dry mass}) = [(M_t - M_d) / (M_d - rM_t)] \cdot 100, \quad (3)$$

$$W_w\,(\%\text{ wet mass}) = \{(M_t - M_d) / [(1 - r)\,M_t]\} \cdot 100, \quad (4)$$

where M_t and M_d are measured in grams.

Bulk Density

Bulk density (ρ) is the density of the total sample including the pore fluid (i.e., $\rho = M_t / V_t$, where V_t is the total sample volume [cm^3]).

Grain Density

Grain density was determined from the dry mass and dry volume measurements. Both mass and volume must be corrected for salt, leading to the following equation:

$$\rho_g = (M_d - M_s) / [V_d - (M_s / \rho_s)], \quad (5)$$

where M_d is the dry mass (g) and ρ_s is the density of salt (2.257 g/cm^3).

$M_s = rM_w$ (g) is the mass of salt in the pore fluid, M_w (g) is the salt-corrected mass of the seawater:

$$M_w = (M_t - M_d)/(1-r). \quad (6)$$

Porosity

Porosity (ϕ) represents the ratio of pore-water volume to total volume expressed as a percentage. The following relationship using calculated grain density, ρ_g, and bulk density ρ was employed:

$$\phi = [(\rho_g - \rho) / (\rho_g - \rho_w)] \cdot 100, \quad (7)$$

where ρ_g represents the grain density, ρ is the bulk density, and ρ_w is the density of seawater.

Dry Density

The dry density is the ratio of the dry mass (M_d) to the total volume (V_t). The dry density was calculated using the corrected water content (W_d) and porosity (ϕ) as follows:

$$\rho_d = (\phi / W_d) \cdot \rho_w. \quad (8)$$

Velocity Measurements

The Hamilton Frame Velocimeter (Hamilton, 1971) was used to measure compressional-wave velocities. Velocity was determined using an impulsive signal with a frequency of 500 kHz. For sediments, velocities were measured in half liners or on discrete samples removed from the core. Crystalline rocks were sampled as minicores (2.54 cm diameter) that were drilled perpendicular to the axis of the core (X-direction). The ends of the minicores were trimmed parallel with a rock saw, and velocities were measured along the axis of the minicore. Distilled water was used as a coupling fluid at the transducer-core interfaces.

The dimensions of samples measured in the Hamilton Frame were determined with digital calipers. Traveltime was estimated by identification of the first break of the stacked waveforms. Traveltime was corrected for system delays and velocities were calculated from the corrected traveltime and path length. Velocity data are reported here in raw form, but corrections for in situ temperature and pressure can also be made using the relationships in Wyllie et al. (1956).

DOWNHOLE MEASUREMENTS

Introduction

Downhole logs are used to continuously measure physical, chemical, and structural properties of formations penetrated by drilling,

thereby complementing discrete core measurements. The data are rapidly collected and interpretation of the continuous in situ measurements allows stratigraphic, lithologic, geophysical, mineralogic, and structural characteristics of the formation to be quantified. When core recovery is incomplete, log data may serve as a proxy for physical properties and sedimentological data and permit the core to be placed in its proper stratigraphic position within the cored interval. Geophysical well-logging is also used to aid in characterization of lithologic sequences when integrated with core and seismic reflection data.

During Leg 173, the triple combination (geophysical) tool string was run at Sites 1065, 1068, and 1069, and the Formation MicroScanner-sonic (FMS-sonic) tool string at Site 1065. Schematic diagrams of these standard tool strings are illustrated in Figure 14.

Principles and Uses of the Tools

The principles of operation and uses of the tools are described in Serra (1984, 1986) and Rider (1996). They are briefly summarized below. The specific depths of investigation into the formation and the vertical borehole resolution are sensor-dependent and are presented in Table 3.

The NGT (Natural Gamma-ray Tool) and HNGS (Hostile Environment Natural Gamma-ray Sonde) measure the natural gamma radiation from isotopes of potassium (K), thorium (Th), and uranium (U) in the rocks surrounding the tool. In sediment, high K and Th values indicate greater clay concentrations, and increased U values often indicate the presence of organic matter. The HNGS and NGT are placed at the top of the triple combination and FMS-sonic tool strings, respectively. Natural gamma-ray data recorded for each run provide a common basis for log correlation and depth adjustment.

The APS (Accelerator Porosity Sonde) emits fast neutrons, which are slowed by hydrogen in the formation, and the energy of the backscattered neutrons is measured. Most hydrogen is in the pore water, hence porosity may be derived. However, hydrogen bound in minerals such as clays also contributes to the measurement, so the raw porosity value is often an over-estimate.

The HLDS (Hostile Environment Litho-Density Sonde) and HLDT (Hostile Environment Litho-Density Tool) emit high-energy gamma rays, which are scattered by the electrons in the formation. The electron density, and hence the bulk density, is derived from the energy of the backscattered gamma rays. Porosity may also be derived from this bulk density, if the matrix density is known. In addition, the PEF (photo-electric effect factor) is measured: photoelectric absorption occurs when the gamma rays reach a low energy (<150 keV) after being continually scattered by the electrons in the formation. The PEF depends on the atomic number of the elements in the formation, thus the magnitude of this measurement is nearly independent of porosity. The HLDS, APS, and HNGS were first used by the ODP on Leg 166 (Eberli, Swart, Malone, et al., 1997).

The TLT (Lamont-Doherty Temperature Logging Tool) is a self-recording, high-resolution temperature tool that can be attached to the bottom of any Schlumberger tool string, except the FMS, to record borehole temperatures. From these data it is possible to identify abrupt temperature gradient changes that may indicate localized fluid flow between the borehole and the formation.

The DIT (Dual Induction Tool) measures the formation resistivity at three different penetration depths, by electromagnetic induction for the deep (ILD) and medium (ILM) resistivity, and by current balancing for the shallow resistivity (SFLU: Spherically Focused Log). Porosity, clay content, fluid salinity, grain-size, and gas hydrate content all contribute to the resistivity.

The SDT (Sonic Digital Tool array) measures the traveltime of sound waves along the borehole wall between transmitters and receivers, over distances of 2.4, 3.0, and 3.6 m. Only compressional-wave velocities are determined on board ship, but the full sonic waveforms are recorded for postcruise processing to determine shear wave and Stoneley wave velocities. The SDT is coupled with the FMS.

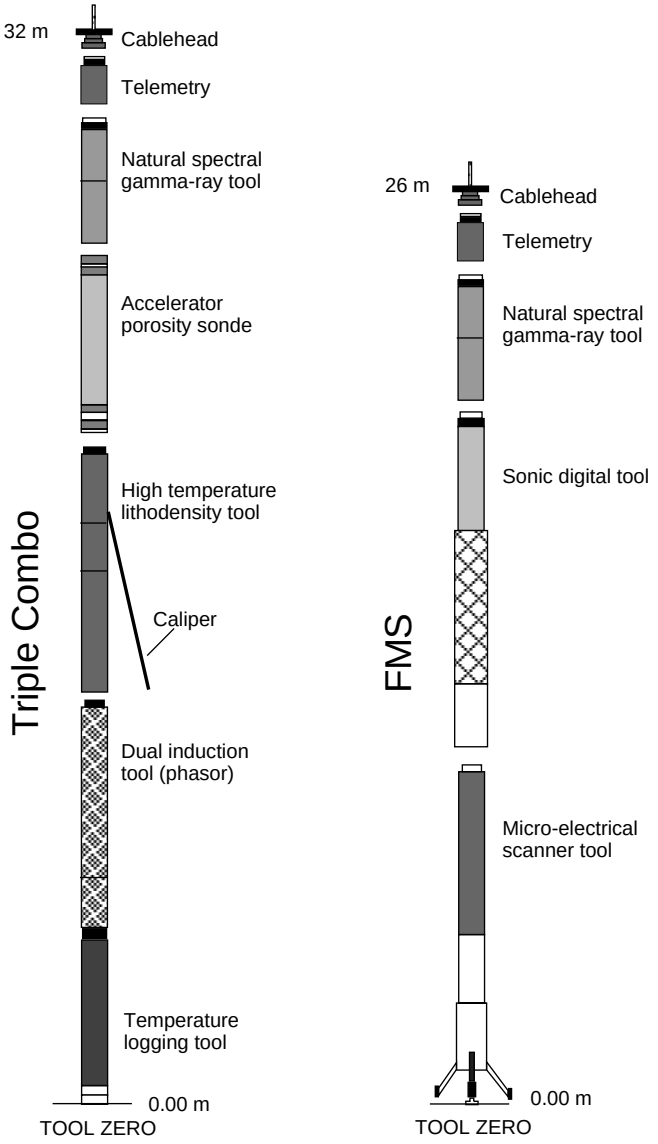

Figure 14. Schematic diagram of the logging tool strings used during Leg 173. Tool strings are not to scale.

The FMS tool produces high-resolution images of the microresistivity of the borehole wall that can be used for detailed sedimentological or structural interpretation. The tool comprises four orthogonal pads, each having 16 button electrodes, that are pressed against the borehole wall (Serra, 1989). Roughly 30% of a 25-cm diameter borehole is imaged. The vertical resolution is ~5 mm, allowing features such as burrows, thin beds, fractures, veins, and foliations to be imaged. The FMS is coupled to a general-purpose inclinometer tool (GPIT), which provides the images with a spatial orientation, so that the azimuth of structures can be obtained for the logged interval. Further processing can provide oriented measurements of the strike and dip of planar features.

Comparison of core images recorded by the CoreScan system (see "Core Imaging" section, this chapter) and microresistivity images obtained with the FMS-sonic tool should enable core-log integration and the determination of true core depth, comparison, and orientation of structural features.

Data Quality

Data quality is largely determined by the state of the borehole wall. If it is irregular, too wide, or if there are many wash-outs, there may be problems with those tools that require good contact with the wall (density, porosity, and FMS). Deep investigation measurements, such as the resistivity and sonic velocity, are least sensitive to borehole conditions. The quality of the borehole is helped by minimizing the circulation of drilling fluid and by logging a young hole or a dedicated hole that has been drilled immediately before logging.

Operations

After coring had finished, the hole was filled with viscous drilling fluid, and the drill-pipe tripped to around 100 mbsf, back to the full depth, and then back to around 100 mbsf when possible, to clean the hole and stabilize the borehole walls. Two tool strings were run sequentially down the hole on wireline cable: the triple combination, which consists of HNGS, APS, HLDS or HLDT, DIT, and TLT, and the FMS combined with the NGT and SDT. A wireline heave compensator was used to minimize the effect of the ship's motion on the tool position.

Data for each logging run were acquired, recorded on disk, and monitored in real time on the Schlumberger Maxis 500 logging computer. Data were transferred to shipboard computers for preliminary interpretation using Schlumberger's GeoFrame software package, and also transmitted to Lamont-Doherty Earth Observatory Borehole Research Group (LDEO-BRG) using the digital high-speed data link of the Inmarsat B satellite communication system.

The LDEO-BRG, Leicester University Borehole Research (LUBR), and the Institut Méditerranéen de Technologie (IMT), in conjunction with Schlumberger Well Logging Services, provided the geophysical well logging aboard the *JOIDES Resolution*.

REFERENCES

Applegate, J.L., and Bergen, J.A., 1988. Cretaceous calcareous nannofossil biostratigraphy of sediments recovered from the Galicia Margin, ODP Leg 103. *In* Boillot, G., Winterer, E.L., et al., *Proc. ODP, Sci. Results*, 103: College Station, TX (Ocean Drilling Program), 293–348.

ASTM, 1989. *Annual Book of ASTM Standards for Soil and Rock: Building Stones* (Vol. 4.08): *Geotextiles:* Philadelphia (Am. Soc. Testing and Mater.).

Bergen, J.A., 1994. Berriasian to early Aptian calcareous nannofossils from the Vocontian Trough (SE France) and Deep Sea Drilling Site 534: new nannofossil taxa and a summary of low-latitude biostratigraphic events. *J. Nannoplankton Res.*, 16:59–69.

Berggren, W.A., Kent, D.V., Swisher, C.C., III, and Aubry, M.-P., 1995. A revised Cenozoic geochronology and chronostratigraphy. *In* Berggren, W.A., Kent, D.V., Aubry, M.-P., and Hardenbol, J. (Eds.), *Geochronology, Time Scales and Global Stratigraphic Correlation*. Spec. Publ.—Soc. Econ. Paleontol. Mineral., 54:129–212.

Blow, W.H., 1979. *The Cainozoic Globigerinida:* Leiden (E.J. Brill).

Boyce, R.E., 1976. Definitions and laboratory techniques of compressional sound velocity parameters and wet-water content, wet-bulk density, and porosity parameters by gravimetric and gamma-ray attenuation techniques. *In* Schlanger, S.O., Jackson, E.D., et al., *Init. Repts. DSDP,* 33: Washington (U.S. Govt. Printing Office), 931–958.

Bukry, D., 1973. Low-latitude coccolith biostratigraphic zonation. *In* Edgar, N.T., Saunders, J.B., et al., *Init. Repts. DSDP,* 15: Washington (U.S. Govt. Printing Office), 685–703.

————, 1975. Coccolith and silicoflagellate stratigraphy, northwestern Pacific Ocean, Deep Sea Drilling Project Leg 32. *In* Larson, R.L., Moberly, R., et al., *Init. Repts. DSDP,* 32: Washington (U.S. Govt. Printing Office), 677–701.

Cande, S.C., and Kent, D.V., 1995. Revised calibration of the geomagnetic polarity timescale for the Late Cretaceous and Cenozoic. *J. Geophys. Res.*, 100:6093–6095.

Cannat, M., Karson, J.A., Miller, D.J., et al., 1995. *Proc. ODP, Init. Repts.*, 153: College Station, TX (Ocean Drilling Program).

Caron, M., 1985. Cretaceous planktic foraminifera. *In* Bolli, H.M., Saunders, J.B., and Perch-Nielsen, K. (Eds), *Plankton Stratigraphy:* Cambridge (Cambridge Univ. Press), 17–86.

Channell, J.E.T., Erba, E., Nakanishi, M., and Tamaki, K., 1995. Late Jurassic–Early Cretaceous time scales and oceanic magnetic anomaly block models. *In* Berggren, W.A., et al. (Eds.), *Geochronology, Time Scales and Global Stratigraphic Correlation.* Spec. Publ.—Soc. Econ. Paleontol. Mineral., 54:51–63.

Comas, M.C., Sánchez-Gómez, M., Cornen, G., and de Kaenel, E., 1996. Serpentinized peridotite breccia and olistrostrome on basement highs of the Iberia Abyssal Plain: implications for tectonic margin evolution. *In* Whitmarsh, R.B., Sawyer, D.S., Klaus, A., and Masson, D.G. (Eds.), *Proc. ODP, Sci. Results,* 149: College Station, TX (Ocean Drilling Program), 577–591.

de Kaenel, E., and Bergen, J.A., 1996. Mesozoic calcareous nannofossil biostratigraphy from Sites 897, 899, and 901, Iberia Abyssal Plain: new biostratigraphic evidence. *In* Whitmarsh, R.B., Sawyer, D.S., Klaus, A., and Masson, D.G. (Eds.), *Proc. ODP, Sci. Results,* 149: College Station, TX (Ocean Drilling Program), 27–59.

DMT-GeoTec/Geo-Engineering, 1996. *DMT Color CoreScan Users Manual. Acquisition and Evaluation Software.*

Eberli, G.P., Swart, P.K., Malone, M.J., et al., 1997. *Proc. ODP, Init. Repts.*, 166: College Station, TX (Ocean Drilling Program).

Erba, E., Premoli Silva, I., and Watkins, D.K., 1995. Cretaceous calcareous plankton biostratigraphy of Sites 872 through 879. *In* Haggerty, J.A., Premoli Silva, I., Rack, F., and McNutt, M.K. (Eds.), *Proc. ODP, Sci. Results*, 144: College Station, TX (Ocean Drilling Program), 157–169.

Gibson, I.L., Milliken, K.L., and Morgan, J.K., 1996. Serpentinite-breccia landslide deposits generated during crustal extension at the Iberia Margin. *In* Whitmarsh, R.B., Sawyer, D.S., Klaus, A., and Masson, D.G. (Eds.), *Proc. ODP, Sci. Results,* 149: College Station, TX (Ocean Drilling Program), 571–575.

Gieskes, J.M., Gamo, T., and Brumsack, H., 1991. Chemical methods for interstitial water analysis aboard *JOIDES Resolution. ODP Tech. Note,* 15.

Gradstein, F.M., Agterberg, F.P., Ogg, J.G., Hardenbol, J., van Veen, P., Thierry, J., and Huang, Z., 1995. A Triassic, Jurassic and Cretaceous time scale. *In* Berggren, W.A., Kent, D.V., and Aubry, M.P. (Eds.), *Geochronology, Time Scales and Global Stratigraphic Correlation.* Spec. Publ.—Soc. Econ. Paleontol. Mineral., 54:95–128.

Hamilton, E.L., 1971. Prediction of in-situ acoustic and elastic properties of marine sediments. *Geophysics*, 36:266–284.

Hoppie, B.W., Blum, P., and the Shipboard Scientific Party, 1994. Natural gamma-ray measurements on ODP cores: introduction to procedures with examples from Leg 150. *In* Mountain, G.S., Miller, K.G., Blum, P., et al., *Proc. ODP, Init. Repts.,* 150: College Station, TX (Ocean Drilling Program), 51–59.

Irvine, T.N., 1982. Terminology for layered intrusions. *J. Petrol.,* 23:127–162.

Keating, B.H., 1984. Magnetometer measurements on the drilling floor of the Glomar Challenger: possible causes of rock remagnetization. In Hay, W.W., Sibuet, J.-C., et al., *Init. Repts. DSDP,* 75: Washington (U.S. Government Printing Office), 1219–1226.

Kennett, J.P., and Srinivasan, M.S., 1983. *Neogene Planktonic Foraminifera: A Phylogenetic Atlas:* Stroudsburg, PA (Hutchinson Ross).

Kvenvolden, K.A., and McDonald, T.J., 1986. Organic geochemistry on the *JOIDES Resolution*—an assay. *ODP Tech. Note,* 6.

Le Bas, M.J., Le Maitre, R.W., Streckeisen, A., and Zanettin, B., 1986. A chemical classification of volcanic rocks based on the total alkali-silica diagram. *J. Petrol.,* 27:745–750.

Manheim, F.T., and Sayles, F.L., 1974. Composition and origin of interstitial waters of marine sediments, based on deep sea drill cores. *In* Goldberg, E.D. (Ed.), *The Sea* (Vol. 5): *Marine Chemistry: The Sedimentary Cycle:* New York (Wiley), 527–568.

Martini, E., 1971. Standard Tertiary and Quaternary calcareous nannoplankton zonation. *In* Farinacci, A. (Ed.), *Proc. 2nd Int. Conf. Planktonic Microfossils Roma:* Rome (Ed. Tecnosci.), 2:739–785.

Martini, E., and Müller, C., 1986. Current Tertiary and Quaternary calcareous nannoplankton stratigraphy and correlations. *Newsl. Stratigr.,* 16:99–112.

Mascle, J., Lohmann, G.P., Clift, P.D., et al., 1996. *Proc. ODP, Init. Repts.*, 159: College Station, TX (Ocean Drilling Program).

Mazzullo, J.M., Meyer, A., and Kidd, R.B., 1988. New sediment classification scheme for the Ocean Drilling Program. *In* Mazzullo, J., and Gra-

ham, A.G. (Eds.), *Handbook for Shipboard Sedimentologists.* ODP Tech. Note, 8:45–67.
Munsell Color Company, Inc., 1971. *Munsell Soil Color Charts:* Baltimore, MD (Munsell).
Ocean Drilling Program, 1996. *Tech Help: a Reference for the Physical Properties Specialist,* Science Services Department, 170.
Okada, H., and Bukry, D., 1980. Supplementary modification and introduction of code numbers to the low-latitude coccolith biostratigraphic zonation (Bukry, 1973; 1975). *Mar. Micropaleontol.,* 5:321–325.
Passchier, C.W., and Trouw, R.A.J., 1996. *Microtectonics:* Berlin (Springer-Verlag).
Perch-Nielsen, K., 1985. Mesozoic calcareous nannofossils. *In* Bolli, H.M., Saunders, J.B., and Perch-Nielsen, K. (Eds.), *Plankton Stratigraphy:* Cambridge (Cambridge Univ. Press), 329–426.
Ramsay, J.G., and Huber, M.I., 1983. *The Techniques of Modern Structural Geology* (Vol. 1): *Strain Analysis:* London (Acad. Press).
————, 1987. *The Techniques of Modern Structural Geology* (Vol. 2): *Folds and Fractures:* London (Academic).
Rider, M., 1996. *The Geological Interpretation of Well Logs:* Caithness (Whittles Publishing).
Robaszynski, F., and Caron, M., 1979. Atlas de foraminifères planctoniques du Crétace moyen (Mer Boréale et Tethys) (Vols. 1 and 2). *Cah. Micropaleontol.*
Robaszynski, F., Caron, M., Gonzales-Donoso, J.-M., Wonders, A.A.H., and the European Working Group on Planktonic Foraminifera, 1984. Atlas of Late Cretaceous globotruncanids. *Rev. Micropaleontol.,* 26:145–305.
Rothwell, R.G., 1989. *Minerals and Mineraloids in Marine Sediments: An Optical Identification Guide:* Basking, UK (Elsevier Appl. Sci. Publ.).
Sass, J.H., Kennelly, J.P., Jr., Smith, E.P., and Wendt, W.E., 1984. Laboratory line-source methods for the measurement of thermal conductivity of rocks near room temperature. *Open-File Rep.—U.S. Geol. Surv.,* 84-0091.
Sawyer, D.S., Whitmarsh, R.B., Klaus, A., et al., 1994. *Proc. ODP, Init. Repts.,* 149: College Station, TX (Ocean Drilling Program).
Serra, O., 1984. *Fundamentals of Well-Log Interpretation* (Vol. 1): *The Acquisition of Logging Data:* Dev. Pet. Sci., 15A: Amsterdam (Elsevier).
————, 1986. *Fundamentals of Well-Log Interpretation* (Vol. 2): *The Interpretation of Logging Data.* Dev. Pet. Sci., 15B.
————, 1989. *Formation MicroScanner Image Interpretation:* Houston (Schlumberger Educ. Services), SMP-7028.
Shipboard Scientific Party, 1988. Site 709. *In* Backman, J., Duncan, R.A., et al., *Proc. ODP, Init. Repts.,* 115: College Station, TX (Ocean Drilling Program), 459–588.
————, 1992. Explanatory notes. *In* Collot, J.-Y., Greene, H.G., Stokking, L.B., et al., *Proc. ODP, Init. Repts.,* 134: College Station, TX (Ocean Drilling Program), 65–91.
————, 1994a. Explanatory notes. *In* Sawyer, D.S., Whitmarsh, R.B., Klaus, A., et al., *Proc. ODP, Init. Repts.,* 149: College Station, TX (Ocean Drilling Program), 11–34.
————, 1994b. Site 897. *In* Sawyer, D.S., Whitmarsh, R.B., Klaus, A., et al., *Proc. ODP, Init. Repts.,* 149: College Station, TX (Ocean Drilling Program), 41–113.
————, 1994c. Site 899. *In* Sawyer, D.S., Whitmarsh, R.B., Klaus, A., et al., *Proc. ODP, Init. Repts.,* 149: College Station, TX (Ocean Drilling Program), 147–209.
————, 1994d. Site 901. *In* Sawyer, D.S., Whitmarsh, R.B., Klaus, A., et al., *Proc. ODP, Init. Repts.,* 149: College Station, TX (Ocean Drilling Program), 263–268.
————, 1997. Explanatory notes. *In* Paull, C.K., Matsumoto, R., Wallace, P.J., et al., *Proc. ODP, Init. Repts.,* 164: College Station, TX (Ocean Drilling Program), 13–41.
————, 1998. Explanatory notes. *In* Keigwin, L., Rio, D., Acton, G., et al., *Proc. ODP, Init. Repts.,* 172: College Station, TX (Ocean Drilling Program), 13–29.
Sissingh, W., 1977. Biostratigraphy of Cretaceous calcareous nannoplankton. *Geol. Mijnbouw,* 56:37–65.
Streckeisen, A., 1976. To each plutonic rock its proper name. *Earth Sci. Rev.,* 12:1–33.
Taira, A., Hill, I., Firth, J.V., et al., 1991. *Proc. ODP, Init. Repts.,* 131: College Station, TX (Ocean Drilling Program).
Toumarkine, M., and Luterbacher, H., 1985. Paleocene and Eocene planktic foraminifera. *In* Bolli, H.M., Saunders, J.B., and Perch-Nielsen, K. (Eds.), *Plankton Stratigraphy:* Cambridge (Cambridge Univ. Press), 87–154.
Vacquier, V., 1985. The measurement of thermal conductivity of solids with a transient linear heat source on the plane surface of a poorly conducting body. *Earth Planet. Sci. Lett.,* 74:275–279.
Von Herzen, R.P., and Maxwell, A.E., 1959. The measurement of thermal conductivity of deep-sea sediments by a needle-probe method. *J. Geophys. Res.,* 64:1557–1563.
Wayne Rasband, 1997. *NIH Image 1.58 Users Manual.* U.S. Nat. Inst. Health.
Weber, H., 1994. Analyse geologischer Strukturen mit einem Bohrkernscanner. *Felsbau,* 12.
Wyllie, M.R.J., Gregory, A.R., and Gardner, L.W., 1956. Elastic wave velocities in heterogeneous and porous media. *Geophysics,* 21:41–70.

Ms 173IR-102

Table 3. Vertical resolution and depth of investigation of the logging tools employed on Leg 173.

Tool string	Tool	Measurement	Sample interval (cm)	Approximate vertical resolution (cm)	Depth of investigation (cm)
Triple combination (total length ~32 m)	HNGS	Natural gamma	15	45	Variable
	APS	Porosity	5 or 15	30	15
	HLDS	Bulk density, PEF	2.5 or 15	15/45	15–60
	HLDT	Resistivity-ILD	2.5 or 15	200	150
	DIT	Resistivity-ILM	2.5 or 15	150	76
		Resistivity-SFLU	2.5 or 15	75	38
	TLT	Temperature	1/s	—	—
FMS-sonic (total length ~26 m)	NGT	Natural gamma	15	45	Variable
	SDT	Sonic velocity	15	120	—
	FMS	Resistivity image	0.25	0.5	5–25

Note: See text for explanations of the acronyms. The vertical resolution, or aperture, is the minimum depth interval for which a representative log measurement can be obtained.

Prior Chapter Contents Next Chapter